



HAL
open science

Functional segmentation of the brain cortex using high model order group ICA

Vesa Kiviniemi, Tuomo Starck, Jukka Remes, Xiang-Yu Long, Juha Nikkinen, Juha Veijola, Irma Moilanen, Marianne Haapea, Yu-Feng Zang, Matti Isohanni, et al.

► **To cite this version:**

Vesa Kiviniemi, Tuomo Starck, Jukka Remes, Xiang-Yu Long, Juha Nikkinen, et al.. Functional segmentation of the brain cortex using high model order group ICA. *Human Brain Mapping*, 2009, 30 (12), pp.3865-n/a. 10.1002/hbm.20813 . hal-00490112

HAL Id: hal-00490112

<https://hal.science/hal-00490112>

Submitted on 8 Jun 2010

HAL is a multi-disciplinary open access archive for the deposit and dissemination of scientific research documents, whether they are published or not. The documents may come from teaching and research institutions in France or abroad, or from public or private research centers.

L'archive ouverte pluridisciplinaire **HAL**, est destinée au dépôt et à la diffusion de documents scientifiques de niveau recherche, publiés ou non, émanant des établissements d'enseignement et de recherche français ou étrangers, des laboratoires publics ou privés.



Functional segmentation of the brain cortex using high model order group ICA

Journal:	<i>Human Brain Mapping</i>
Manuscript ID:	HBM-08-0444.R2
Wiley - Manuscript type:	Research Article
Date Submitted by the Author:	01-Apr-2009
Complete List of Authors:	Kiviniemi, Vesa; Oulu University Hospital, Diagnostic Radiology Starck, Tuomo; Oulu University Hospital, Radiology Remes, Jukka; Oulu University Hospital, Radiology Long, Xiang-Yu; Beijing Normal University, State Key Laboratory of Cognitive Neuroscience Nikkinen, Juha; Oulu University Hospital, Radiology Veijola, Juha; Oulu University Hospital, Psychiatry Moilanen, Irma; Oulu University Hospital, Child Psychiatry Haapea, Marianne; Oulu University Hospital, Radiology; Oulu University Hospital, Psychiatry Zang, Yu-Feng; Beijing Normal University, State Key Laboratory of Cognitive Neuroscience and Learning Isohanni, Matti; Oulu University Hospital, Psychiatry Tervonen, Osmo; Oulu University Hospital, Radiology
Keywords:	ICA, fMRI, resting state, brain cortex



Functional segmentation of the brain cortex using high model order group PICA.

Kiviniemi Vesa¹, Starck Tuomo¹, Jukka Remes¹, Xiangyu Long^{1,2}, Nikkinen Juha¹, Haapea Marianne^{1,3}, Veijola Juha³, Moilanen Irma⁴, Matti Isohanni³, Yu-Feng Zang², Tervonen Osmo¹

¹Department of Diagnostic Radiology, Oulu University Hospital

²State Key Laboratory of Cognitive Neuroscience, Beijing Normal University, China

³Department of Psychiatry, Oulu University Hospital

⁴Department of Child Psychiatry, Oulu University Hospital

Abstract: Baseline activity of resting state brain networks (RSN) in a resting subject has become one of the fastest growing research topics in neuroimaging. It has been shown that up to 12 RSNs can be differentiated using an independent component analysis (ICA) of the blood oxygen level dependent (BOLD) resting state data. In this study, we investigate how many RSN signal sources can be separated from the entire brain cortex using high dimension ICA analysis from a group dataset. Group data from 55 subjects was analysed using temporal concatenation and a probabilistic ICA (PICA) algorithm. ICA repeatability testing (ICASSO) verified that 60 of the 70 computed components were robustly detectable. Forty-two independent signal sources were identifiable as RSN, and 28 were related to artifacts or other non-interest sources (non-RSN). The depicted RSNs bore a closer match to functional neuroanatomy than the previously reported RSN components. The non-RSN sources have significantly lower temporal inter-source connectivity than the RSN ($p < 0.0003$). We conclude that the high model order ICA of the group BOLD data enables functional segmentation of the brain cortex. The method enables new approaches to causality and connectivity analysis with more specific anatomical details.

Introduction

Since the discovery of functionally connected low frequency fluctuations of the blood oxygen dependent (BOLD) with a functional MRI by Biswal and colleagues, the detection of baseline activity within functional brain networks has become a fast growing interest area in brain imaging research [Biswal et al., 1995; Fox & Raichle 2007, Vincent et al., 2007]. Intra-cortical local field potential and multiunit activity fluctuations partly correlate with the fluctuations of the BOLD signal with a 6 second lag in anesthetized conditions [Logothetis et al., 2001; Shmuel et al., 2008]. In addition to electrophysiological activity, metabolic, and vasomotor effects partly explain the detected BOLD fluctuation changes [Fukunaga et al., 2008; Kannurpatti et al., 2008; Kiviniemi 2008].

The combined effects of these fluctuations in neuronal networks have been shown to be differentiable from noise during normal, awake resting conditions. Independent component analysis (ICA) is an effective tool in separating statistically independent source signals of the BOLD data. ICA separates various sources of the fMRI signal by maximizing the non-Gaussianity of the source signals. Spatial domain ICA (sICA) can separate BOLD signal sources that represent reactions to externally cued task-activations, background activity within functional brain (i.e. resting state) networks (RSN), and various physiological noise and artifact sources [Beckmann et al., 2004 & 2005; Calhoun et al., 2001; Kiviniemi et al., 2003; McKeown et al., 1998; Van de Ven 2004]. ICA methodology yields results that are equally accurate to other contemporary methods of detecting large scale temporally coherent networks from the BOLD signal data [Long et al., 2008].

1
2
3
4
5
6 It has been suggested that 10 to 12 RSNs can be detected from the brain cortex from resting state
7
8 BOLD data, using ICA with a component dimensionality, i.e. a model order, around 25-40
9
10 components [Beckmann et al. 2005, De Luca et al., 2006, Damoiseaux et al., 2006]. However,
11
12 the most recent reports on topographic delineation of cortex and functional connectivity nodes
13
14 show that there should be more than a dozen detectable functional networks on the brain cortex
15
16 [Bartels & Zeki 2005; Cohen et al., 2008; Di Martino et al., 2008; Malinen et al., 2007, Mezer et
17
18 al., 2008; Pawela et al., 2008]. When the model order of the ICA estimation is increased, the
19
20 separated BOLD signal sources have been shown to split into several functional nodes [Li et al.,
21
22 2007; Ma et al., 2007, Malinen et al., 2007, Eichele et al., 2008]. McKeown and co-workers have
23
24 shown that the detected ICA components of BOLD data actually represent deterministic signal
25
26 sources of the data, even in very high model orders [McKeown et al., 2002].
27
28
29
30
31
32
33

34 In this study, we evaluate how many independent RSN signal sources of baseline brain activity
35
36 can be detected from the brain cortex using a fairly large group of subjects and a relatively high
37
38 order group ICA. We show that the previously detected RSN signal sources can be differentiated
39
40 into a more finely tuned functional anatomy by extending the use of temporal connectivity, the
41
42 frequency power spectral and the anatomical clustering characteristics of the signal sources into
43
44 group analysis data. We show that over 60 of the detected signal sources can be robustly detected
45
46 with repeatability analysis (ICASSO-software package) from group data. We found supporting
47
48 evidence for our hypothesis that true RSN sources have increased temporal inter-source
49
50 connectivity compared to noise sources. Spatial overlap of the RSN components, and predefined
51
52
53
54
55
56
57
58
59
60

1
2
3 anatomical structures are presented. The possible functional and clinical implications of the
4
5 results are discussed.
6
7
8
9

10 **Materials and Methods**

11
12
13
14

15 The ethical committee of Oulu University Hospital has approved the studies for which the
16
17 subjects have been recruited, and informed consent has been obtained from each subject
18
19 individually according the Helsinki declaration. Fifty-five control subjects were chosen (age
20
21 24.96 ± 5.25 years, 32 ♀, 23 ♂) from three resting state studies: an At Risk Mental Stage
22
23 (ARMS) 1986 birth cohort study of ADHD and schizophrenia; a 1966 birth cohort study of
24
25 schizophrenia; brain tumor resting state study, total $n = 200$. Subjects were imaged on a GE 1.5T
26
27 HDX scanner equipped with an 8-channel head coil using parallel imaging with an acceleration
28
29 factor 2. The scanning was done during January 2007- May 2008. All subjects received identical
30
31 instructions: to simply rest and focus on a cross on an fMRI dedicated screen which they saw
32
33 through the mirror system of the head coil. Hearing was protected using ear plugs, and motion
34
35 was minimized using soft pads fitted over the ears.
36
37
38
39

40 The functional scanning was performed using an EPI GRE sequence. The TR used was 1800 ms
41
42 and the TE was 40 ms. The whole brain was covered, using 28 oblique axial slices 4 mm thick
43
44 with a 0.4 mm space between the slices. FOV was 25.6 cm x 25.6 cm with a 64 x 64 matrix, and
45
46 a flip angle of 90 degrees. The resting state scan consisted of 253 functional volumes. The first
47
48 three images were excluded due to T1 equilibrium effects. In all three studies, the resting state
49
50 scanning started the protocols, and lasted 7 minutes and 36 seconds. In addition to resting-state
51
52 fMRI, T1-weighted scans were taken with 3D FSPGR BRAVO sequence (FOV 24.0 cm, matrix
53
54
55
56
57
58
59
60

1
2
3 256 x 256, slice thickness 1.0 mm, TR 12.1ms, TE 5.2 ms, and flip angle 20 degrees) in order to
4
5 obtain anatomical images for co-registration of the fMRI data to standard space coordinates.
6
7

8 9 10 **Pre-processing of imaging data**

11
12
13
14
15 Head motion in the fMRI data was corrected using multi-resolution rigid body co-registration of
16
17 volumes, as implemented in FSL 3.3 MCFLIRT software [Jenkinson et al. 2002]. The default
18
19 settings used were: middle volume as reference, a three-stage search (8 mm rough + 4 mm,
20
21 initialized with 8 mm results + 4 mm fine grain, initialized with the previous 4 mm step results)
22
23 with final tri-linear interpolation of voxel values, and normalized spatial correlation as the
24
25 optimization cost function. Brain extraction was carried out for motion corrected BOLD volumes
26
27 with optimization of the deforming smooth surface model, as implemented in FSL 3.3 BET
28
29 software [Smith 2002] using threshold parameters $f = 0.5$ and $g = 0$; and for 3D FSPGR volumes,
30
31 using parameters $f = 0.25$ and $g = 0$. After brain extraction, the BOLD volumes were spatially
32
33 smoothed, 7 mm FWHM Gaussian kernel and voxel time series were detrended using a Gaussian
34
35 linear high-pass filter with a 125 second cutoff. The FSL 4.0 fslmaths tool was used for these
36
37 steps.
38
39

40
41
42
43 Multi-resolution affine co-registration as implemented in the FSL 4.0 FLIRT software
44
45 [Jenkinson et al. 2002] was used to co-register mean non-smoothed fMRI volumes to 3D FSPGR
46
47 volumes of corresponding subjects, and 3D FSPGR volumes to the Montreal Neurological
48
49 Institute (MNI) standard structural space template (MNI152_T1_2mm_brain template included
50
51 in FSL). Tri-linear interpolation was used, a correlation ratio was used as the optimization cost
52
53 function, and regarding the rotation parameters a search was done in the full $[-\pi \pi]$ range. The
54
55
56
57
58
59
60

1
2
3 resulting transformations and the tri-linear interpolation were used to spatially standardize
4 smoothed and filtered BOLD volumes to the 2 mm MNI standard space. Because an sICA was
5 run later on fMRI data concatenated from the 55 subjects, in practice the spatial resolution of
6 spatially standardized BOLD volumes had to be lowered to 4 mm.
7
8
9
10
11

12 13 14 15 **Spatial domain analysis** 16

17
18
19 Analysis was carried out using Probabilistic Independent Component Analysis (PICA)
20 [Beckmann et al., 2004] on pre-processed and spatially standardized BOLD data, temporally
21 concatenated from data sets of individual subjects. The implementation of PICA and temporal
22 concatenation in FSL 4.0 MELODIC software was used in this study. The default processing
23 provided in MELODIC, and used in this study, starts on the subject level. Intensities of voxel
24 time courses in pre-processed fMRI volumes are converted to percentages of change with respect
25 to the mean intensity in those voxels. This is followed by group level joined normalization of
26 voxel time course variances. The mean 4D fMRI data set is averaged from individual data sets,
27 and the variance estimate is computed from it. The variance estimate used in normalization is
28 computed so that 1) data with respect to its time points (temporal dimensions) is whitened, 2) in
29 whitened space, large values corresponding to variance, possibly not originating from Gaussian
30 processes, are noted with some threshold value, and their influence excluded from data in the
31 original space, after which 3) variance is computed ordinarily on resulting residual data. Within
32 MELODIC implementation and in its joined normalization scheme, this threshold value was set
33 to 3.1. Fourth, voxels with insufficient variances (<0.0001) are set to zero because they contain
34 nearly constant time courses, and in that sense a bad signal-to-noise ratio that would (after
35
36
37
38
39
40
41
42
43
44
45
46
47
48
49
50
51
52
53
54
55
56
57
58
59
60

1
2
3 variance normalization) contribute too much to the analysis. Each individual subject fMRI data
4
5 set is divided voxel-wise with a standard deviation corresponding to the voxel-wise variance
6
7 estimate. A whitening matrix corresponding to the whitening mean 4D fMRI data set is
8
9 computed and used for group-level joint whitening and dimensionality reduction of each
10
11 individual subject fMRI data sets. The number of resulting dimensions corresponds to the model
12
13 order of ICA that is intended to be used. In this study, the model order was chosen to be 70, in
14
15 correspondence to the high order sICA modeling of the resting state BOLD data. Since PPCA
16
17 estimation suggested 73 components in an initial test, we reduced it to 70 components due to
18
19 better extraction of extracranial voxels after using a more sensitive BET algorithm outside the
20
21 MELODIC framework.
22
23
24
25
26
27
28

29 The jointly whitened and reduced individual fMRI data sets are further whitened, and then
30
31 temporally concatenated. Further dimensionality reduction is performed with principal
32
33 components analysis (PCA) on the concatenated data. The number of dimensions in the
34
35 concatenated data (number of subjects times 70) is reduced to the number of independent
36
37 components to be computed, 70 in this study. Finally, FastICA [Hyvärinen 1999] is performed
38
39 using voxel values as samples, and PCA reduced and whitened temporal dimensions as variables.
40
41 In this study, we used the default settings in the MELODIC software: symmetric
42
43 orthogonalization and skewness (“pow3”) as the contrast function.
44
45
46
47
48
49

50 In a PICA framework, estimated intensity maps (independent components) are converted to Z-
51
52 scores by dividing intensity values by voxel-wise standard deviations of noise distribution.
53
54

55 Standard deviations are estimated through calculation of corresponding voxel-wise variances of
56
57
58
59
60

1
2
3 the original pre-processed data in the subspace left out by dimensionality reduction steps.
4
5 Probability distributions of values in individual resulting score maps are modeled using a
6
7 mixture of functions, a zero mean Gaussian function and two gamma functions. The Gaussian
8
9 function corresponds to the effects due to chance, and the gamma functions model outliers not
10
11 observed by chance. For a given Z-score, the sum of gamma function values divided by the sum
12
13 of all function values can be used to calculate the probability of actually observing an effect with
14
15 that score. With regard to these probabilities, a probability threshold (P-value) is set to leave out
16
17 (set to zero) those voxel values in score maps that are presumed to be observed in the PICA
18
19 results by chance. In this study, we used $P = 0.5$, attributing equal relevance to both false
20
21 negatives and false positives.
22
23
24
25
26
27
28

29 The Juelich histological atlas [Eickhoff et al. 2007], and the Harvard -Oxford cortical and
30
31 subcortical atlases (Harvard Center for Morphometric Analysis) which are provided with the
32
33 FSL4 software package were used to quantify anatomical characteristics of thresholded Z-score
34
35 maps. For this purpose, maps were upsampled back to 2 mm resolution MNI standard space.
36
37 Individual anatomical regions in the probabilistic atlases were binarized, and used as masks to
38
39 extract the corresponding regions in maps. An FSL4 fslstats tool was used to calculate mean and
40
41 maximum intensity in regions, as well as the location of maximum intensity. The number of
42
43 voxels in the masked PICA maps was also calculated, and divided by number of voxels in the
44
45 whole anatomical masking region, to provide a percentage of the coverage of different
46
47 anatomical areas by individual maps.
48
49
50
51
52
53
54
55
56
57
58
59
60

1
2
3 A neuroradiologist (VK) depicted the thresholded PICA maps corresponding to the RSNs by
4 choosing anatomically clustered sources in the cortical regions, in the vicinity of functional brain
5 regions. The sources were further classified into three regions for illustration purposes with a
6 scheme modified from Salvador and co-workers [2005] (peri-sylvian = rolandic and temporal,
7 frontal, occipito-parietal). In each of the selected sources, 1) sources presented clustered voxel
8 groups, 2) sources were focused on cortical structures, and 3) time courses in the ICA mixing
9 matrix corresponding to the maps showed elevated low frequency (<0.1 Hz) power. Artifactual
10 non-RSNs were identified based on their motion related location at the borders of the brain, in
11 cerebrospinal fluid (CSF), at the proximity of large blood vessels, in white matter, and in the
12 vicinity of areas shown to be susceptible to physiological pulsations with relatively increased or
13 mixed high frequency power [Birn et al., 2006; Lund et al., 2006].
14
15
16
17
18
19
20
21
22
23
24
25
26
27
28
29
30
31

32 **Repeatability analysis:** The data from the final step prior to FastICA was also subjected to ICA
33 repeatability analysis (ICASSO) [Himberg, Hyvärinen & Esposito 2004]. Since ICA is sensitive
34 to its initialization, this framework runs FastICA multiple times on the same data, with random
35 initializations and clusters with a hierarchical clustering algorithm, on the results from individual
36 runs. The number of clusters is the same as the number of components, and provides statistics
37 about the quality of the clusters, reflecting the stability of the ICA results. In this study, we used
38 the provided Matlab implementation [Himberg, Hyvärinen & Esposito 2004] with 100 runs, and
39 a low epsilon threshold (0.0000001) so that optimization would not converge too soon before
40 reaching extrema. Symmetric orthogonalization and skewness (“skew”) as the contrast function
41 were also used in this setting. The conservative cluster quality index I_q was used to estimate
42 individual component repeatability [Himberg, Hyvärinen & Esposito 2004]. I_q is one for an ideal
43
44
45
46
47
48
49
50
51
52
53
54
55
56
57
58
59
60

1
2
3 cluster, and decreases when component clusters become less compact and isolated in repeated
4
5 ICA runs.
6
7
8
9

10 **Time domain analysis**

11
12
13
14
15 A mixing matrix estimated in an sICA contains time courses corresponding to estimated spatial
16
17 maps (independent components). The time courses represent the behavior of non-artifact
18
19 components in time more accurately than the average BOLD time courses computed from the
20
21 same spatial area as in the maps; this is because the most dominant effects of cardiac, respiratory,
22
23 CSF-pulsation and motion, and other artifacts are eliminated into separate components. This
24
25 offers preprocessed time courses for temporal correlation analysis of BOLD signal sources [Jafri
26
27 et al., 2008; Sorg et al., 2007].
28
29
30

31
32 In a temporal concatenation scheme, the mixing matrix can be divided into subject specific
33
34 consecutive segments, reflecting subject-wise temporal behavior of components. In this study,
35
36 these subject specific 250 point time courses were used to assess pair-wise inter component
37
38 connectivity on the group level. The time courses were first de-trended, and then correlated with
39
40 each other on the subject level with the Pearson product-moment correlation coefficient with a
41
42 zero lag. The group level average and standard deviation of the results were calculated for each
43
44 correlation pair's absolute values.
45
46

47
48 In addition, the mean of these group-level absolute correlation coefficients was calculated per
49
50 component within the group of components corresponding to RSNs, and within the group
51
52 corresponding to non-RSNs. These values were tested for differences with a two-sample t-test
53
54
55 between RSNs and non-RSNs.
56
57
58
59
60

Frequency domain analysis

The subject-wise time courses extracted from the mixing matrix were (after detrending) also converted to power spectra, to assess contribution of low frequency power in them. For each time course, a spectrogram was computed with 128-point rectangular windowing in Matlab (R2008a) with the similarly named function. Rectangular windowing was sufficient, since no sinc-interpolation (e.g. no zero padding) was used in the Discrete Fourier Transform. The absolute values of the resulting 123 spectra were raised to the second power to approximate power spectra, and they were averaged to obtain a final power spectrum estimate for each time course.

For the group-level analysis, each power spectrum was normalized by dividing its values by its total power. Normalized power spectra from individual subjects were averaged for each component, to produce a group-level representation of temporal power. In addition, Singular Value Decomposition was used for each component to produce, on a group-level, a rank-1 approximation of subject-specific power spectra for that component. Rank-1 approximation depicts frequencies with the most commonly elevated power in subject-level time courses.

Results

Repeatability measures

An ICASSO algorithm was run on the pre-whitened PCA-data matrix provided by the MELODIC. After 100 repeated runs of the group ICA, significantly clustered components were detected. Fifty-one of the 70 ICs had an I_q over 0.8, and 60 ICs still had an I_q of at least 0.7. Figure 1 shows clustering of the centroid components and stability indexes in reducing the stability order. PICA estimation of the group data yielded 73 components. We made 7 separate runs altering the basic spatial smoothing parameters (3-7mm FWHM), temporal high (100-420 s) and low-pass filtering. In essence, the spatial correlation between the detected ICA components of separate runs was always > 0.7 .

< Fig.1 can be here >

RSN-identification

The group PICA separated 42 components that were identified as RSN. These 42 components cover most of the brain cortex excluding areas having susceptibility artefacts due to air sinuses. The corresponding RSN components had an average $I_q = 0.83 (\pm 0.13)$ in the ICASSO analysis. The RSN components had elevated low frequency fluctuation power and, spatially, were clustered components located in the cortex. Figures 2 to 4 show fused maps and separate spatial distributions of 25 of the different signal sources on both sides of the Sylvian fissure and the

1
2
3 central sulcus (Peri-Sylvian), in the frontal lobe (Frontal), and in the occital and parietal regions
4
5 (Occipito-Parietal). The remaining signal sources are shown in Fig. 5 in more optimal 3D
6
7 presentations.
8
9

10 Twenty-eight ICs were related to non-RSN sources. Eighteen non-RSN components were
11 identified as motion/realignment artifacts, and physiological noise sources such as arterial and
12 CSF pulsation. Ten of the discarded components were detected as large voxel clusters in the
13 white matter, and were not further analysed. Ten examples of the non-RSN sources are shown in
14 Fig.6.
15
16
17
18
19
20
21
22
23
24

25 **Anatomical parcellation**

26
27
28
29 In practice, most of the cerebral cortex can be shown to be segmented with the IC components
30 (c.f. the upper rows in Figures 2-4). On average, the *maximal* spatial correlation between
31 detected RSN components and other sources was 0.2 (sd 0.04). This can be seen in Figures 2-4
32 as a limited spatial overlap of separate signal source components. Table 1 lists the first 3-5
33 largest overlapping *anatomical* segments used in FSL4 (Juelich and Oxford atlases) in
34 comparison with the selected RSN signal sources. The RSN components actually show more
35 connectivity nodes to multiple other anatomical structures, and the complete table is presented in
36 the supplementary material (Supplementary: Extended Table 1.2). In the following, the
37 individual RSN sources are evaluated, based on spatial overlap with pre-existing anatomical
38 segments. Temporal inter-source synchrony of the sources, and the highest spatial correlation
39 with ICASSO components are also presented.
40
41
42
43
44
45
46
47
48
49
50
51
52
53
54
55
56
57
58
59
60

Rolandic signal sources

Figure 2 shows six signal sources identified as peri-rolandic, situated at or in the vicinity of the central sulcus. Although most of the sources have strong localized connectivity, some have long range connectivity to other primary and secondary sensory areas, such as to the visual and auditory regions.

The motor cortex was divided into two different signal sources resembling the classical separation of upper cortical structures representing the hand areas (IC 27) and midline feet areas (IC 19). Similar to the original discovery of Biswal et al., there was a midline connectivity node posterior to the typical SMA seen during activation studies [Biswal et al., 1995]. Another motor cortex component, IC 24, was depicted, but it was not clear whether such parcellation is due to physiological factors, or if the results are split due to positioning differences in the original BOLD axial slices. Anterior to motor areas there were unilateral components (IC's 53 & 60) with positive connectivity to the cerebellum. The right anterior motor IC 60 was spatially larger than the left IC 53.

Primary and secondary somatosensory cortices were separated into signal sources of their own (IC 6 and, 43, respectively). Posterior to these, there was a symmetrical, bilateral post-somatosensory cluster (Figure 5, IC 40). The somatosensory signal source also showed smaller clusters of connectivity to anatomical visual, auditory and Broca's areas (c.f. Table 1_2 [supplementary]). The signal source IC 14 was situated below the somatosensory cortex in the white-grey matter boundary. The secondary somatosensory source (IC 43) also showed

1
2
3 connectivity with structures in the cerebellum, in addition to secondary somatosensory, auditory,
4
5 motor and pre-motor anatomical structures. The supplementary motor area (SMA, i.e.
6
7 juxtapositional lobule) area had bilateral connectivity clusters in IC 49, primarily involving the
8
9 insular cortices, and partly involving the secondary somatosensory area, resembling mirror
10
11 neuron networks. Interestingly, both pre-motor areas BA6 also presented unilateral components,
12
13 i.e. IC's 53 & 60 (Fig 5). There was a tendency that the farther a source was from the central
14
15 sulcus, the longer the distances were between detected connectivity clusters.
16
17
18
19
20
21

22 < Fig 2 can be here >
23

24 **Temporal lobe signal sources**

25
26
27
28
29 In figure 2, the primary auditory cortex was identified as a bilateral component of its own, with a
30
31 right brain dominance (IC 25). As with the peri-rolandic sources, this large network presented
32
33 connectivity with other sources in distant regions, in both the motor and visual areas. A Broca's
34
35 area on the left and an homologous right hemisphere Broca's area were detected in a unique
36
37 bilateral component, with a clear, functionally connected cluster in the right paracingulate areas,
38
39 posterior cingulate gyrus, and bilateral occipital poles (IC 30). The the fronto-insular cortex of
40
41 the salience network was detected in a bilateral IC 15 with a partial Broca's area and inferior
42
43 frontal gyrus involvement, in addition to paracingulate gyrus connectivity [Shihadran et al.,
44
45 2008]. IC 49 showing connectivity to SMA could be differentiated from the salience network.
46
47
48
49 The temporal poles (IC 13, Fig. 5) were also detected in a unique signal source, with
50
51 connectivity to midline structures to bilateral hippocampi.
52
53
54
55
56
57
58
59
60

Frontal signal sources

The frontal lobe had eleven RSN signal sources, seven of which are presented in Figure 3. In five sources (ICs 7, 10, 18, 31 and 37), connectivity to language-related areas, such as the auditory cortex, inferior frontal gyrus and/or Broca's anatomical areas, was detected. In addition to these areas, IC 7 and 10 were also connected to the anterior cingulate and paracingulate gyri. IC 7 had connectivity to the angular gyri and the visual cortex. IC 10 was present at the lower frontal pole and medial frontal cortex, and IC 8 was related to the upper frontal pole, and the middle and superior frontal and angular gyri. IC 18 was connected to the superior frontal gyrus, paracingulate, and cingulate gyri. IC 23 was connected to the angular and supramarginal gyri, along with the visual cortex. IC 37 was related to the superior and medial frontal gyri, and the paracingulate gyri.

< Fig.3 can be here >

Occipital and Parietal signal sources

There were seven separated signal source clusters in the occipital lobe, all spatially connected to visual areas (c.f. Figure 4). IC 2 was situated at the lateral part of the primary visual cortex (V1), as in the lateral visual component in previous papers. Above and lateral to it was IC 4, with midline connectivity in V5. IC 39 was also comprised of bilateral V5 areas, yet different V5 areas from those in IC 4, with connectivity to V1&2 and the inferior and medial temporal gyrus. IC 59 typically presented the previously detected medial visual resting state network, comprising almost completely of the intracalcarine and supracalcarine cortex, the lingual cortex, and the

1
2
3 major parts of V1&2 and the cuneal cortex. An anterior medial visual component IC 32 in V2,
4
5 with hippocampal and geniculate body connectivity, was also detected. A posterior component
6
7 IC 21 was separated from the medial central IC 59. The cuneal and precuneal cortex were
8
9 dominant in IC 63, along with V1&2, with clear retrosplenial connectivity. In addition, there
10
11 were two anti-correlated components in the visual areas (IC's 52 & 61) showing positive z-
12
13 scores caudally on the other visual cortex, and negative z-scores on the contra-lateral side more
14
15 cranially.
16
17
18
19

20 < Fig. 4-6 can be here >
21

22 **Default mode and frontal attention control sources** 23

24
25
26
27 Several ICA sources were detected in the areas known to be related to the default mode network
28
29 (DMN). IC 10 = ventromedial prefrontal cortex (vmPFC), IC 38 = precuneus & parietal lobule
30
31 (PCC). ICs 7, 10, 23, 18, and 37 were closely related to anatomical structures of the DMN (c.f.
32
33 Figures 3-4). The regions usually detected as anti-correlated to DMN in correlation analysis were
34
35 also detected as sources of their own, i.e. IC's 6, 40 and 49 [Fox et al., 2007, Buckner et al.,
36
37 2008]. IC 17 resembles the frontal areas central executive network [Shihadran et al., 2008].
38
39 Figure 7 shows an example of PICA images calculated with 100 repeated ICASSO runs with
40
41 model orders 10, 70 and 150. Please note how the core areas of the default mode divide into
42
43 smaller sub-networks with increasing model order.
44
45
46
47
48
49
50
51
52
53
54

55 < Fig. 7 can be here >
56
57
58
59
60

Time domain synchrony

The inter-source connectivity between all the calculated ICs are presented in a matrix in Figure 8. The graph shows how the individual sources are connected to the other sources on average with zero time lag. The correlation coefficients range from 0.64 to -0.66 (± 0.21). The mean correlation coefficients of each component provide an overall assessment of general inter-source connectivity of a given IC. The overall connectivity of the non-RSN sources was statistically significantly lower than the connectivity of the RSN sources ($t = 4.6$, $p < 0.000024$, c.f. Figure 8 bottom). Eight out of the ten lowest values of summed correlation were depicted in non-RSN sources. There is, however, some overlap in the correlation values between the RSN and non-RSN sources, and temporal zero-lagged correlation alone cannot be used to separate the sources with absolute certainty.

< Fig.8 can be here >

Frequency domain

The mean power spectra of the individual ICA time courses extracted from the group data mixing matrix had increased low frequency power with $1/f$ distribution characteristics (see also Figures 2-4). The first rank approximate of the power spectra shows the most contributing frequencies, mostly presenting the same proportional distribution as the mean power spectra. In the majority of the components, the dominant feature is the $1/f$ characteristic trend. However, in ICs 7, 18, 19, 21, 25, 27, 30, 32, 38, 43, 59, and 63, there is a distinct peak in lower frequencies. That is, the lowest frequency is not with the largest power. The peaks were almost absent from frontal sources, with the exception of DFM related IC 18. Primary auditory IC 25,

1
2
3 somatosensory IC 43, motor ICs 19 and 27, and visual sources 21, 32 and 59 showed peaks. In
4
5 the visual cortex, IC 59 in the medial areas had an exceptional 0.045 Hz frequency peak at the
6
7 most dominant approximate. Default mode IC 38 and the Broca area source IC 30 also presented
8
9 peaks in their power spectra.
10
11

12 **Discussion**

13
14
15
16
17 The results of this study represent functional segmentation of the human brain cortex, using the
18
19 statistical independence of spontaneous brain activity sources as a delineating feature. We have
20
21 shown that the intrinsic baseline activity of the brain cortex can be separated into 42 independent
22
23 sources, having resting state network features, using a high model order PICA approach. These
24
25 sources cover virtually the whole brain cortex, excluding the sources affected by susceptibility
26
27 artefacts near air-sinus interfaces. The dominant low frequency power characteristics of rank-1
28
29 approximates in the RSN support the idea that the sources represent low frequency background
30
31 activity of the RSN. All of the RSN sources have increased LFF power in the mean power
32
33 spectra (c.f. Figures 2-4).
34
35
36
37
38
39
40

41 The utilization of continuous *in vivo* baseline activity information on brain activity offers a
42
43 complementary method to previous anatomical/histological dissection studies, as well as imaging
44
45 data-based segmentation studies, which currently form the basis of spatial localization schemes.
46
47 The introduction of functional segmentation offers a more accurate tool for delineating
48
49 functional activity that traverses presently used tissue segmentation borders in connected
50
51 neuronal networks. In addition, these IC source maps can be used as data driven, statistically
52
53 independent, functional seed regions for further correlation analyses.
54
55
56
57
58
59
60

1
2
3
4
5
6 Using present 1.5 T MRI scanning methodology our group has identified 42 signal sources over
7
8 the whole brain cortex. The results of this study are in excellent agreement with the recent results
9
10 of Cohen et al. [2008], who showed several small functionally connected areas within the same
11
12 cortical regions. The work of Malinen and co-workers convincingly shows that during natural
13
14 stimuli there are all together at least twenty task and non-task related signal sources detectable in
15
16 the brain [Malinen et al., 2007]. Compared to a higher resolution fMRI scan on a rat, the results
17
18 of this study seem conservative, since rats were shown to have some 20 connectivity hubs
19
20 detectable in the somatosensory and visual systems alone [Pawela et al., 2008]. Two groups have
21
22 been able to identify separate regions from the striatum and thalamus with distinct functional
23
24 connectivity to the brain cortex in human subjects [DiMartino et al., 2008, Mezer et al, 2008].
25
26 On a sub-millimeter scale, anatomical structures of the visual field columns and cortical layers
27
28 can be identified based on the spontaneous electrophysiological activity of sub-second time
29
30 scales. This suggests that an even greater number of spontaneous signal sources will be
31
32 detectable with increased spatiotemporal accuracy in the future [Kenet et al., 2003; Pelled &
33
34 Goelman 2004].
35
36
37
38
39
40
41
42

43 The previously detected 12 signal sources that were found in smaller datasets are basically
44
45 summations of some of the sources presented here [Beckmann, et al., 2005; Damoiseaux et al.,
46
47 2006; Sorg et al., 2007; Jafri et al., 2008]. An example of this can be seen in the Figure 7, where
48
49 the DMN is initially presented as one single source with the model order 10, and, after increasing
50
51 the model order, becomes divided into several sources. It seems that low model orders provide
52
53 information on large scale networks, whereas higher model orders, at least in group-data settings,
54
55
56
57
58
59
60

1
2
3 provide sub-network accuracy. We are currently analyzing the effect of model order on the
4
5 dividing of RSN's into sub-networks. We suggest that the 42 group-PICA signal sources
6
7 depicted in this study represent a more finely-tuned and segmented version of the functional
8
9 neuro-anatomy of the RSN's in the brain cortex, and therefore we strongly support using high
10
11 model order in large group datasets.
12
13
14
15
16

17
18 The distinction of components into two categories of either RSN or non-RSN may be somewhat
19
20 arbitrary although there have been some successful attempts towards automated noise removal
21
22 that basically also delineates IC's into neuronal and artifactual originated ones [De Martino et al.,
23
24 2007; Tohka et al., 2008]. One might justifiably speculate in the absence of definite exclusion
25
26 criteria that there exist a "borderline" between RSN sources and non-RSN sources. Some IC's
27
28 have features of cortical signal source overlapping with regions often presenting artifacts. For
29
30 example IC's 3, 24 and 40 all are situated within the cranial brain cortex and somewhat resemble
31
32 sources seen in individual ICA results as motion artefact/partial volume effects. However at least
33
34 IC 40 seems to be a RSN based on further studies not shown here. On the other hand IC's 8, 52
35
36 and 61 are situated very close to sagittal or transverse sinuses and one might speculate that the
37
38 source has some contribution from pulsation from sagittal sinus. However the sagittal sinus at
39
40 least was shown to have an even more confined source of its own (IC 46) c.f. Fig 6. It would be
41
42 beneficial to obtain a more quantitative criteria than anatomical positioning and low frequency
43
44 fluctuation of the sources in order to differentiate true RSN sources from artefacts.
45
46
47
48
49
50
51
52

53 The signal sources depicted here accurately follow the known functional anatomy of the sensory
54
55 and motor networks. Sources IC 19 and 27 together cover 89 % of the right and 86 % of the left
56
57
58
59
60

1
2
3 primary motor cortices when compared to MNI atlases in fsl4. Primary sensorimotor areas were
4
5 shown to have spatial connectivity with fourteen IC's, twelve of which were the same (IC
6
7 3,4,6,14,19,24,27,40,43,53,60,66). The M1 anatomical area was uniquely connected to IC's 41 &
8
9 45 , while S1 was connected to IC 9 & 35, c.f. Table 1_2 in the supplement. Somatosensory S1
10
11 had a spatial overlap of 61 % (IC 6) and S2 72 % (IC 43). The supplementary motor area (i.e.
12
13 juxtapositional lobule) activity was differentiated from the primary sensorimotor components,
14
15 although it was shown to have connectivity to them. SMA was shown to be connected to 12
16
17 RSN's, the largest share being detected in IC 49 (58%). Also IC's 53 (24 %), IC 60 (34%), IC 18
18
19 (30%), IC 19 (36%) had relatively high spatial overlaps with the SMA template. The unilateral
20
21 and somewhat anterior pre-motor sources (IC's 53 & 60: Broadman area BA6, 42 % and 55%,
22
23 respectively) could be related functional differences of the subjects pre-motor areas [Longcamp
24
25 et al, 2005].
26
27
28
29
30
31
32
33

34 Visual sources are separated into multiple sources, and not only into medial and lateral
35
36 components as before. The primary and secondary visual cortices V1 & V 2 were detected in 10
37
38 IC's (IC's 1,2,4,21,32,38,52,59,61,63),and, the largest overlap for V1 was in IC's 21 and 55,
39
40 both having 55.5 %. The secondary V2 had the largest overlaps in IC's 21 (51%) and IC 59
41
42 (54%). The multiple components have a strong resemblance to natural viewing (V1-V5, lateral
43
44 occipital complexes) and listening-related components in the occipital and temporal regions
45
46 [Bartels & Zeki 2005, Malinen et al., 2007]. The positive/negative IC's 52 and 61 resemble
47
48 visual fields seen in visual hemifield activation study using the frequency based group ICA
49
50 [Calhoun et al., 2003].
51
52
53
54
55
56
57
58
59
60

1
2
3 IC 25 was most overlapping with the primary auditory cortex (90.5% with the right TE 1.0 and
4
5 89.7 % with TE 1.2 on the left) and is left-dominant. The primary auditory cortex was connected
6
7 to ten IC's (IC's 1,15,18,25,29,37,39,43,47,68). Broca's area had connectivity with sixteen
8
9 sources (IC's 3,4,7,8,9,10,15,30,31,35,37,39,43,49,66,68) with largest nodes in IC 30 (77 % right
10
11 side), IC 35 (97 % left side). Several other frontal and temporal sources have interesting and
12
13 complex connectivity with various functional regions related to attention, language and other
14
15 cognitive functions. Their spatial overlapping with presently known anatomical regions are rich,
16
17 just like those of the primary sensory and motor cortices, and they are presented more precisely
18
19 in the Supplement: Extended Table 1.2.
20
21
22
23
24
25
26

27 Recent findings show that the DMN nodes have separate causality and connectivity
28
29 characteristics [Sridharan et al., 2008; Uddin et al., 2008]. Also researchers using ICA have
30
31 noticed the separation of the DMN into at least two sub-networks [Calhoun et al., 2008;
32
33 Damoiseaux et al., 2006]. The results of this study shows that the DMN is functionally
34
35 differentiated into anterior and posterior parts. There are also "DMN-type" components (IC 7,
36
37 10, 23, 18, and 37) with clear spatial overlap with DMN related areas [Buckner et al, 2008]. The
38
39 detection of these areas is particularly sensitive to model order of the ICA and we are currently
40
41 investigating this phenomenon.
42
43
44
45
46
47

48 The regions detected as anti-correlated with the DMN in correlation analyses using global mean
49
50 regression were also detected as sources of their own (IC's 6, 40, 49). The use of ICA avoids the
51
52 problematic regression of the global mean signal, although the PCA mean subtraction step in
53
54 pre-processing of PICA also alters the data to some extent [Murphy et al., 2008]. Based on the
55
56
57
58
59
60

1
2
3 present results, the areas anti-correlated to DMN in correlation analyses are also present as
4
5 independent signal sources and therefore may not be completely a by-product of global mean
6
7 signal regression of BOLD signal.
8
9

10
11
12 In order to maximize the chances of effective treatment, it is crucially important to identify
13
14 diseases at the earliest stage possible. Functional alterations often present themselves as
15
16 symptoms prior to irreversible tissue damage. For clinical brain research, function-based tissue
17
18 segmentation is of pivotal importance in the early detection and characterization of diseases.
19
20 Greicius and co-workers [2004, 2007] have already shown that minimally impaired memory
21
22 deficiency or depression are related to the function of a brain network. ICA analyses detecting
23
24 multiple brain networks have shown that, while some networks show no changes, others may be
25
26 more affected by diseases such as Alzheimer's and schizophrenia [Calhoun et al., 2008; Jafri et
27
28 al., 2008; Sorg et al., 2007]. The high model order ICA segmentation increases functional and
29
30 anatomical specificity in the connectivity analysis of the networks and so may enhance our
31
32 ability to detect disease-related network alterations.
33
34
35
36
37
38
39
40

41 The ICA methodology in this study is widely used by other researchers, and we suggest that the
42
43 relatively high number of detected RSN components is due to increased signal-to-noise ratio
44
45 related to the large dataset used in the group analysis. How inter-subject variance affects the
46
47 results is, however, an important question; are we seeing more fringe components that are only
48
49 present on sub-populations within the group [Schmidthorst & Holland, 2004]? For example,
50
51 bored, anxious or enthusiastic subjects might have different strengths of fluctuations in default
52
53
54
55
56
57
58
59
60

1
2
3 mode sub-networks. The answer to this problem is also related to model order of a large group
4 dataset and therefore this issue may not be entirely handled within the scope of this manuscript.
5
6
7
8
9

10 The only minor alteration compared to general trends in ICA analyses was the utilization of 70
11 components. The high model order is supported by the works of McKeown et al. [2002] and
12 some recent ones as well [De Martino et al., 2007, Malinen et al., 2007]. One can always
13 speculate on the effects of over-fitting in the detected components, if there are any. It should be
14 noted that model order estimation with PPCA also yielded high model order numbers, i.e. 73 in
15 this dataset, which strongly speaks against major overfitting. Two of the original 73 components
16 were related to non-accurate extra-brain tissue removal, and this was corrected by utilizing
17 another bet-algorithm outside the MELODICA automated tool.
18
19
20
21
22
23
24
25
26
27
28
29
30
31

32 In order to validate the stability of the method, we employed ICASSO on the pre-processed
33 MELODIC data matrix. In doing so, 60 out of 70 components were shown to have a stability
34 value of at least 0.7 in the group analysis, especially when the ICASSO was computed using a
35 low epsilon threshold. Higher epsilon thresholds led to less clustered components in repeated
36 runs due to less demanding convergence of the ICA algorithm around local maxima. It should be
37 interesting to see how the repeated ICASSO analysis results differentiate from single subject run
38 PICA results. We are currently exploring the benefits of using both PICA and ICASSO in a
39 combined analysis setting. Another unclear issue is how the RSN's detected in the group data
40 can be used in individual settings. Based on the results shown here, a familiar ICA related issue
41 re-emerges; what is the optimal model order of ICA in datasets with increased subject numbers,
42 and how are pre-processing schemes influencing the results? We are currently investigating
43
44
45
46
47
48
49
50
51
52
53
54
55
56
57
58
59
60

1
2
3 whether it is still possible to detect more accurate RSN components with bigger data samples and
4
5 higher model orders.
6
7
8
9

10 The temporal correlation matrix of the ICA enables the assessment of connectivity between all
11 the detected signal sources. It can be seen that some of the sources have limited correlation to
12 practically all the other sources, which becomes visible as a dark row in the mean connectivity
13 matrix (c.f. Figure 5). These dark lines tend to be non-RSNs sources related to noise/artefacts
14 and, indeed, their mean *temporal* inter-source connectivity is significantly lower than those of
15 the RSN sources. The temporal correlation structure could perhaps be used as a feature in
16 differentiating the non-RSN and RSN sources with different lag periods. The non-RSN sources
17 are thus temporally more *independent* than the connected RSN sources, and therefore their
18 automated separation seems feasible from this point of view [De Martino et al., 2007; Tohka et
19 al., 2008].
20
21
22
23
24
25
26
27
28
29
30
31
32
33
34
35

36 There have been concerns about the uncontrolled nature of the resting state regarding attention
37 and free thinking induced alterations. In this study, we used a semi-resting state by instructing
38 the subject to fixate on a cross shown on the screen. The subject is not completely at rest and
39 tries to sustain attention on the cross. On the other hand, no restrictions on the fixation or mental
40 imagery were given either. The fixation reduces motion artefacts and still offers some cognitive
41 baseline function in order to reduce some of the variability of free thinking. McAvoy et al
42 recently presented rather similar spatial distribution of areas where BOLD fluctuation frequency
43 is dependent on whether the subject has eyes open, closed or is fixating on a cross. We found a
44 similar distribution of areas, and in addition differences in power spectral densities between the
45
46
47
48
49
50
51
52
53
54
55
56
57
58
59
60

1
2
3 visual area sources. The V1 related medial (IC 59) and dorsal (IC 21) components in this study
4
5 have somewhat different rank-1 approximates from the other occipital sources. It would be
6
7 interesting to see how these sources differ in subjects with eyes closed in a large number of
8
9 subjects.
10
11

12
13
14
15 Importantly, it has been shown that the effective estimation and removal of underlying
16
17 oscillations significantly improves the signal-to-noise ratio in the task activation studies [Fox et
18
19 al., 2006]. In addition, baseline activity oscillations preceding stimuli explains the major share
20
21 of the subsequent stimulus response variability [Boly et al., 2007; Fox et al., 2006, Eichele et al.,
22
23 2008]. There may be stimulus-locked connectivity alterations that can be masked by the baseline
24
25 oscillations, rendering the hemodynamic response functions and correlation based connectivity
26
27 measurement inaccurate. After establishing the cortical oscillatory activity within each of the
28
29 networks with high model order ICA, one may be able to utilize these baseline oscillations in a
30
31 regression analysis in a more accurate manner, and obtain increased signal-to-noise ratios in
32
33 stimulus related effective connectivity analyses of brain networks. Also, due to the fact that ICA
34
35 separates noise sources, the mixing matrix signals seem to yield effective measures for
36
37 connectivity and causality measurements, without biasing physiological or motion related
38
39 correlations [Eichele, et al.2008, Sorg et al., 2008, Calhoun et al., 2008].
40
41
42
43
44
45
46
47

48
49 Mantini and co-workers were able to distinguish EEG power distribution fingerprints of
50
51 different RSNs [Mantini et al., 2007]. Although the frequency resolution of fMRI alone is not as
52
53 good as that of EEG, one is able to depict differences between the power distributions and first
54
55 rank approximates of the RSNs (c.f. Figures 2-4). Primary sensory and motor sources, default
56
57
58
59
60

1
2
3 mode, Broca's area and some occipital visual sources present some prominent frequency peaks
4
5 in addition to the 1/f trend in the spectrum. The frontal sources predominantly have 1/f
6
7 distributions without clear peaks. The functional significance of this difference in peak frequency
8
9 distributions needs further elucidation.
10
11

12 13 14 15 **Conclusion**

16
17
18
19
20 The brain cortex can be robustly segmented into 42 independent RSNs by utilizing the group-
21
22 ICA of baseline BOLD data. This method offers complementary information on tissue
23
24 characteristics of cortical structures compared to previous post-mortem histological and
25
26 microanatomic dissection of structures. Utilization of a relatively high model order and multi-
27
28 subject group data enables increased accuracy of functional segmentation of brain tissue due to
29
30 increased signal-to-noise ratio. The method reveals multiple interlinked connectivity sub-
31
32 networks enabling more fine-tuned characterization of seed regions for further causality and
33
34 connectivity analyses.
35
36
37
38
39
40

41 **Grants:** Finnish Academy-Chinese NSFC Collaboration NEURO-program grant # 117111,
42
43 Finnish Medical Foundation, and Finnish Neurological Association grants were used in the
44
45 production of this research.
46
47
48
49

50 **Acknowledgements:** The authors cordially thank Dr. Christian Beckmann for his assistance in
51
52 PICA mixing matrix and bet analyses, and, Dr Gordon Roberts for editorial assistance. The
53
54
55
56
57
58
59
60

1
2
3 authors would also like to express their deep gratitude to the reviewers and handling editor for
4
5 their excellent suggestions and corrections on the manuscript.
6
7
8
9

10 **References**

11
12
13
14
15 Bartels A, Zeki S (2005): The chronoarchitecture of the cerebral cortex. *Philos Trans R Soc*
16
17 *Lond B Biol Sci.* 360(1456):733-50.
18
19

20
21
22 Beckmann CF, Smith SM (2004): Probabilistic independent component analysis for functional
23
24 magnetic resonance imaging. *IEEE Trans Med Imaging.* 23(2):137-52.
25
26
27

28
29 Beckmann CF, DeLuca M, Devlin JT, Smith SM (2005): Investigations into resting-state
30
31 connectivity using independent component analysis. *Philos Trans R Soc Lond B Biol Sci.*
32
33 29:360(1457):1001-13.
34
35
36
37

38
39 Biswal BB, Yetkin FZ, Haughton VM, Hyde JS (1995): Functional connectivity in the motor
40
41 cortex of resting human brain using echo-planar MRI. *Magn Reson Med* 34:537-541.
42
43
44

45
46 Birn RM, Diamond JB, Smith MA, Bandettini PA. (2006): Separating respiratory-variation-
47
48 related fluctuations from neuronal-activity-related fluctuations in fMRI. *Neuroimage.*
49
50 15;31(4):1536-48.
51
52
53
54

55 Boly M, Balteau E, Schnakers C, Degueldre C, Moonen G, Luxen A, Phillips C, Peigneux P,
56
57
58
59
60

1
2
3 Maquet P, Laureys S. (2007): Baseline brain activity fluctuations predict somatosensory
4 perception in humans. Proc Natl Acad Sci 17;104(29):12187-92.
5
6
7

8
9
10 Calhoun VD, Adali T, Pearlson GD, Pekar JJ (2001): A method for making group inferences
11 from functional MRI data using independent component analysis, Hum Brain Map 14(3):140–
12 151.
13
14
15

16
17
18 Calhoun VD, Adali T, Pekar JJ, Pearlson GD (2003): Latency (in)sensitive ICA. Group
19 independent component analysis of fMRI data in the temporal frequency domain.
20 Neuroimage. 20(3):1661-9
21
22
23
24
25
26

27
28
29 Calhoun VD, Kiehl KA, Pearlson GD (2008): Modulation of temporally coherent brain networks
30 estimated using ICA at rest and during cognitive tasks. Hum Brain Mapp. 29(7):828-38.
31
32
33
34
35

36
37 Cohen AL, Fair DA, Dosenbach NU, Miezin FM, Dierker D, Van Essen DC, Schlaggar BL,
38 Petersen SE (2008): Defining functional areas in individual human brains using resting
39 functional connectivity MRI. NeuroImage 15;41(1):45-57.
40
41
42
43
44

45
46 Damoiseaux JS, Rombouts SA, Barkhof F, Scheltens P, Stam CJ, Smith SM, Beckmann CF
47 (2006) Consistent resting-state networks across healthy subjects. Proc Natl Acad Sci
48 12;103(37):13848-53.
49
50
51
52
53
54
55
56
57
58
59
60

1
2
3 De Martino F, Gentile F, Esposito F, Balsi M, Di Salle F, Goebel R, Formisano E (2007):
4
5 Classification of fMRI independent components using IC-fingerprints and support vector
6
7
8 machine classifiers NeuroImage, Volume 34 (1):177-194.
9

10
11
12 De Luca M, Beckmann CF, De Stefano N, Matthews PM, Smith SM (2006): fMRI resting state
13
14 networks define distinct modes of long-distance interactions in the human brain. Neuroimage.
15
16
17 29(4):1359-67.
18
19

20
21
22 Di Martino A, Scheres A, Margulies DS, Kelly AM, Uddin LQ, Shehzad Z, Biswal B, Walters
23
24 JR, Castellanos FX, Milham MP (2008): Functional Connectivity of Human Striatum: A Resting
25
26 State fMRI Study. Cereb Cortex. 18(12):2735-47.
27
28

29
30
31 Eichele T, Debener S, Calhoun VD, Specht K, Engel AK, Hugdahl K, von Cramon DY,
32
33 Ullsperger M (2008): Prediction of human errors by maladaptive changes in event-related brain
34
35 networks. Proc Natl Acad Sci 105:6173-6178.
36
37

38
39
40 Eickhoff SB, Paus T, Caspers S, Grosbras MH, Evans AC, Zilles K, Amunts K (2007):
41
42 Assignment of functional activations to probabilistic cytoarchitectonic areas revisited.
43
44
45 NeuroImage, 36(3): 511-521.
46
47

48
49
50 Fox MD, Snyder AZ, Zacks JM, Raichle ME (2006): Coherent spontaneous activity accounts for
51
52 trial-to-trial variability in human evoked brain responses. Nat Neurosci. 9(1):23-5.
53
54
55
56
57
58
59
60

1
2
3 Fox MD, Raichle ME (2007): Spontaneous fluctuations in brain activity observed with
4 functional magnetic resonance imaging. *Nat Rev Neurosci.* 8(9):700-11.
5
6
7

8
9
10 Fukunaga M, Horovitz SG, de Zwart JA, van Gelderen P, Balkin TJ, Braun AR, Duyn JH
11 (2008): Metabolic origin of BOLD signal fluctuations in the absence of stimuli. *J Cereb Blood*
12 *Flow Metab.* 28(7):1377-87.
13
14
15

16
17
18
19
20 Greicius MD, Srivastava G, Reiss AL, Menon V (2004): Default-mode network activity
21 distinguishes Alzheimer's disease from healthy aging: Evidence from functional MRI. *Proc Natl*
22 *Acad Sci* 101(13):4637-4642.
23
24
25

26
27
28
29 Greicius MD, Flores BH, Menon V, Glover GH, Solvason HB, Kenna H, Reiss AL, Schatzberg
30 AF (2007): Resting-state functional connectivity in major depression: abnormally increased
31 contributions from subgenual cingulate cortex and thalamus. *Biol Psychiatry.* 62(5):429-37.
32
33
34
35

36
37
38
39 Himberg J, Hyvärinen A, Esposito F (2004): Validating the independent components of
40 neuroimaging time series via clustering and visualization. *Neuroimage* 22(3):1214-22.
41
42
43

44
45
46 Hyvärinen, A (1999): Fast and Robust Fixed-Point Algorithms for Independent Component
47 Analysis. *IEEE Trans. on Neural Networks,* 10(3):626-634,
48
49
50

1
2
3 Jafri MJ, Pearlson GD, Stevens M, Calhoun VD (2008): A method for functional network
4 connectivity among spatially independent resting-state components in schizophrenia.
5
6 Neuroimage. 15;39(4):1666-81.
7
8
9

10
11
12 Jenkinson M, Bannister PR, Brady JM, Smith SM (2002): Improved optimisation for the robust
13 and accurate linear registration and motion correction of brain images. NeuroImage, 17(2):825-
14
15 841.
16
17
18
19

20
21
22 Kannurpatti SS, Biswal BB, Kim YR, Rosen BR (2008): Spatio temporal characteristics of low
23 frequency BOLD signal fluctuations in isoflurane anesthetized rat brain. NeuroImage
24
25 40(4):1738-47.
26
27
28
29

30
31
32 Kenet T, Bibitchkov D, Tsodyks M, Grinvald A, Arieli A (2003): Spontaneously emerging
33 cortical representations of visual attributes. Nature 425(6961):954-6.
34
35
36
37

38
39 Kiviniemi V, Kantola J-H, Jauhiainen J, Hyvärinen A, Tervonen O (2003): Independent
40 Component Analysis of Non-deterministic fMRI Signal Sources. NeuroImage 19:253-260.
41
42
43
44

45 Kiviniemi V (2008): Endogenous brain fluctuations and diagnostic imaging.
46
47

48 Hum Brain Mapp. 2008 Jul;29(7):810-7. Review
49
50
51
52
53
54
55
56
57
58
59
60

1
2
3 Kleinfeld D, Mitra PP, Helmchen F, Denk W 1998. Fluctuations and stimulus-induced changes
4 in blood flow observed in individual capillaries in layers 2 through 4 of rat neocortex. Proc Natl
5 Acad Sci 95:15741-15746.
6
7

8
9
10
11
12 Li YO, Adali T, Calhoun VD (2007): Estimating the number of independent components for
13 functional magnetic resonance imaging data. Hum Brain Mapp. (11):1251-66.
14
15

16
17
18
19
20 Logothetis NK, Pauls J, Augath M, Trinath T, Oeltermann A (2001): Neurophysiological
21 investigation of the basis of the fMRI signal. Nature 412:150-157.
22
23

24
25
26
27 Long XY, Zuo XN, Kiviniemi V, Yang Y, Zou QH, Zhu CZ, Jiang TZ, Yang H, Gong QY,
28 Wang L, Li KC, Xie S, Zang YF (2008): Default mode network as revealed with multiple
29 methods for resting-state functional MRI analysis. J Neurosci Methods. 30;171(2):349-55.
30
31
32

33
34
35
36 Longcamp M, Anton JL, Roth M, Velay JL (2005): Premotor activations in response to visually
37 presented single letters depend on the hand used to write: a study on left-handers.
38
39
40
41 Neuropsychologia. 43(12):1801-9.
42
43

44
45
46 Lund TE, Madsen KH, Sidaros K, Luo WL, Nichols TE (2006): Non-white noise in fMRI: does
47 modelling have an impact? Neuroimage 29(1):54-66.
48
49

50
51
52
53 Ma L, Wang B, Chen X, Xiong J (2007): Detecting functional connectivity in the resting brain: a
54 comparison between ICA and CCA. Magn Reson Imaging. 25(1):47-56.
55
56
57
58
59
60

1
2
3
4 Malinen S, Hlushchuk Y, Hari R (2007): Towards natural stimulation in fMRI--issues of data
5 analysis. *NeuroImage* 35:131-139.
6
7

8
9
10 Mantini D, Perrucci MG, Del Gratta C, Romani GL, Corbetta M. (2007): Electrophysiological
11 signatures of resting state networks in the human brain. *Proc Natl Acad Sci* 7;104(32):13170-5.
12
13

14
15
16
17 McAvoy M, Larson-Prior L, Nolan TS, Vaishnavi SN, Raichle ME, d'Avossa G (2008) Resting
18 states affect spontaneous BOLD oscillations in sensory and paralimbic cortex. *Journal of*
19
20
21
22
23
24
25
26
27
28
29
30
31
32
33
34
35
36
37
38
39
40
41
42
43
44
45
46
47
48
49
50
51
52
53
54
55
56
57
58
59
60

Neurophysiology 100:922-931.

McKeown MJ, Jung TP, Makeig S, Brown G, Kindermann SS, Lee TW, Sejnowski TJ (1998):
Spatially independent activity patterns in functional MRI data during the stroop color-naming
task. *Proc Natl Acad Sci* 95(3):803-10.

McKeown MJ, Varadarajan V, Huettel S, McCarthy G. (2002): Deterministic and stochastic
features of fMRI data: implications for analysis of event-related experiments. *J Neurosci*
Methods. 118(2):103-13.

Mezer A, Yovel Y, Pasternak O, Gorfine T, Assaf Y. (2008) Cluster analysis of resting-state
fMRI time series. *Neuroimage*. doi:10.1016/j.neuroimage.2008.12.015

1
2
3 Murphy K, Birn RM, Handwerker DA, Jones TB, Bandettini PA.(2008) The impact of global
4 signal regression on resting state correlations: Are anti-correlated networks introduced?
5
6 Neuroimage. [epub ahead of print].
7
8
9

10
11
12
13
14 Onton J, Westerfield M, Townsend J, Makeig S (2006) Imaging human EEG dynamics using
15 independent component analysis. *Neurosci Biobehav Rev* 30:808-822.
16
17

18
19
20
21 Pawela CP, Biswal BB, Cho YR, Kao DS, Li R, Jones SR, Schulte ML, Matloub HS, Hudetz
22 AG, Hyde JS (2008): Resting-state functional connectivity of the rat brain. *Magn Reson Med*.
23
24 59(5):1021-9.
25
26
27

28
29
30 Pelled G, Goelman G (2004): Different physiological MRI noise between cortical layers. *Magn*
31
32 *Res Med* 52:913-916
33
34

35
36
37 Salvador R, Suckling J, Coleman MR, Pickard JD, Menon D, Bullmore E (2005):
38
39 Neurophysiological architecture of functional magnetic resonance images of human brain. *Cereb*
40
41 *Cortex* 15(9):1332-42.
42
43
44

45
46
47 Schmithorst VJ, Holland SK (2004) Comparison of three methods for generating group statistical
48
49 inferences from independent component analysis of functional magnetic resonance imaging data.
50
51 *J Magn Reson Imaging* 19:365-368.
52
53
54
55
56
57
58
59
60

1
2
3 Shmuel A, Leopold DA (2008): Neuronal correlates of spontaneous fluctuations in fMRI signals
4
5 in monkey visual cortex: Implications for functional connectivity at rest. Hum Brain Mapp.
6
7
8 29(7):751-61.
9

10
11
12 Smith SM. (2002): Fast robust automated brain extraction. Human Brain Mapping, 17(3):143-
13
14 155,
15
16

17
18
19 Sorg C, Riedl V, Mühlau M, Calhoun VD, Eichele T, Läer L, Drzezga A, Förstl H, Kurz A,
20
21 Zimmer C, Wohlschläger AM (2007): Selective changes of resting-state networks in individuals
22
23 at risk for Alzheimer's disease. Proc Natl Acad Sci 104(47):18760-5.
24
25
26

27
28
29 Sridharan D, Levitin DJ, Menon V (2008): A critical role for the right fronto-insular cortex in
30
31 switching between central-executive and default mode networks. Proc Natl Acad Sci
32
33 105(34):12569-12574.
34
35

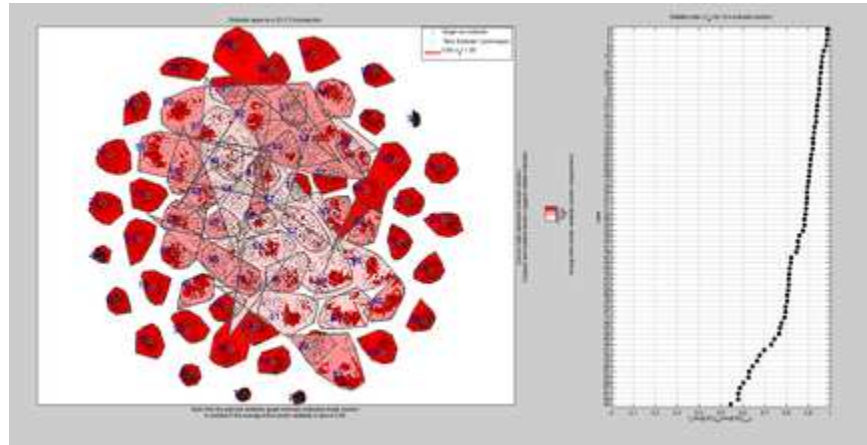
36
37
38 Tohka J, Foerde K, Aron AR, Tom SM, Toga AW, Poldrack RA (2008): Automatic independent
39
40 component labeling for artifact removal in fMRI. Neuroimage. 39(3):1227-45.
41
42
43

44
45
46 Uddin LQ, Clare Kelly AM, Biswal BB, Xavier Castellanos F, Milham MP (2008): Functional
47
48 connectivity of default mode network components: Correlation, anticorrelation, and causality.
49
50 Hum Brain Mapp. *epub ahead of print*
51
52
53
54
55
56
57
58
59
60

1
2
3 van de Ven VG, Formisano E, Prvulovic D, Roeder CH, Linden DE (2004): Functional
4 connectivity as revealed by spatial independent component analysis of fMRI measurements
5 during rest. Hum Brain Mapp.22(3):165-78.
6
7
8
9

10
11
12 Vincent JL, Patel GH, Fox MD, Snyder AZ, Baker JT, Van Essen DC, Zempel JM, Snyder LH,
13 Corbetta M, Raichle ME (2007) Intrinsic functional architecture in the anaesthetized monkey
14 brain. Nature 447:83-86.
15
16
17
18
19
20
21
22
23
24
25
26
27
28
29
30
31
32
33
34
35
36
37
38
39
40
41
42
43
44
45
46
47
48
49
50
51
52
53
54
55
56
57
58
59
60

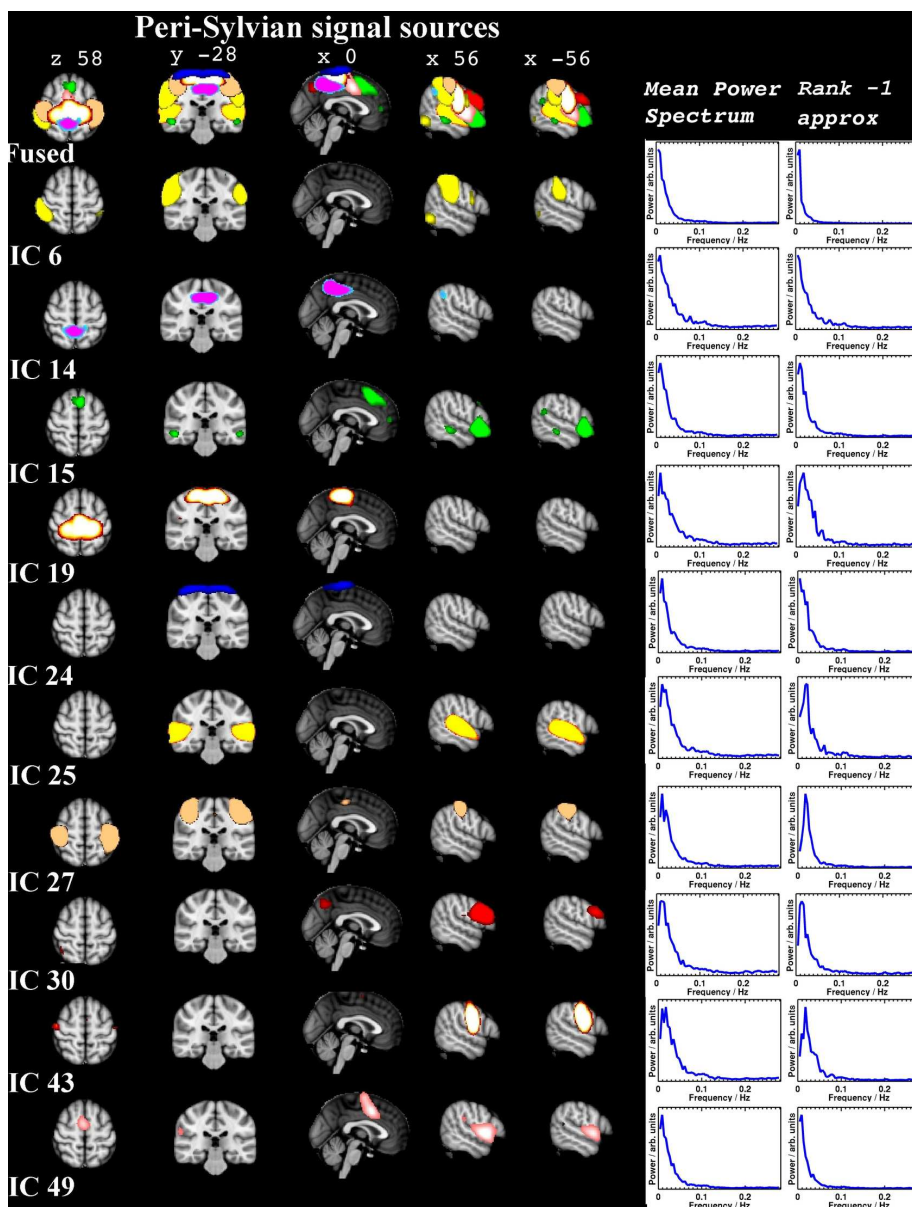
For Peer Review



On the left, the clustering of group PICA-derived components in ICASSO after 100 repeated runs. On the right, ICASSO run components in descending clustering index values, showing that in 60/70 components the clusters are repeatedly detectable ($I_q \geq 0.7$). Please note that the ICASSO cluster numbers are not the same as the PICA numbers in the text and other images.

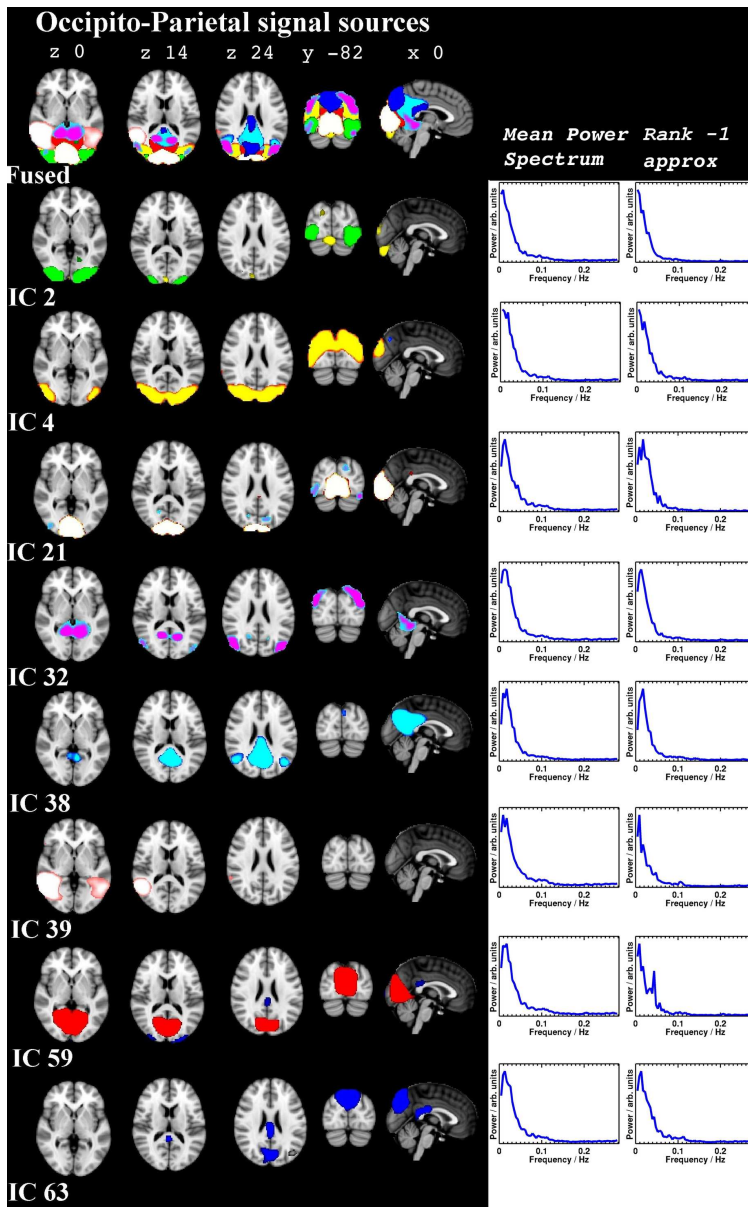
18x9mm (600 x 600 DPI)

1
2
3
4
5
6
7
8
9
10
11
12
13
14
15
16
17
18
19
20
21
22
23
24
25
26
27
28
29
30
31
32
33
34
35
36
37
38
39
40
41
42
43
44
45
46
47
48
49
50
51
52
53
54
55
56
57
58
59
60



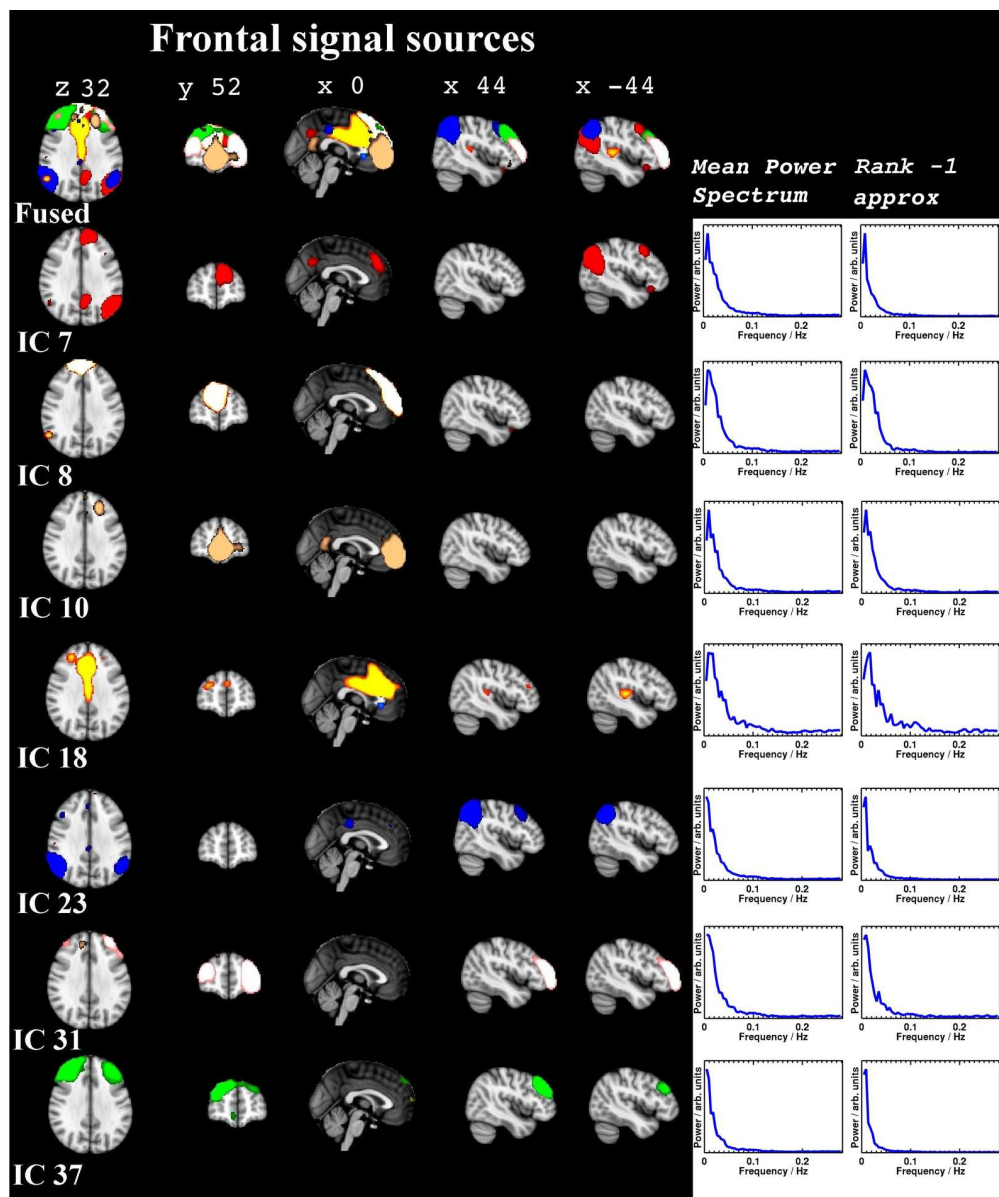
Signal sources located around the Sylvian fissure, both peri-rolandic and temporal sources are presented. At the top, a fused image presenting overlays of the different sources. Below that, IC sources are mapped with color labels provided by the fsl-view tool. On the right, the mean power spectra and rank 1 approximate on the same row as the map of the given source. On the left, the sources are numbered using the same numbers as referenced in the text.

71x93mm (600 x 600 DPI)



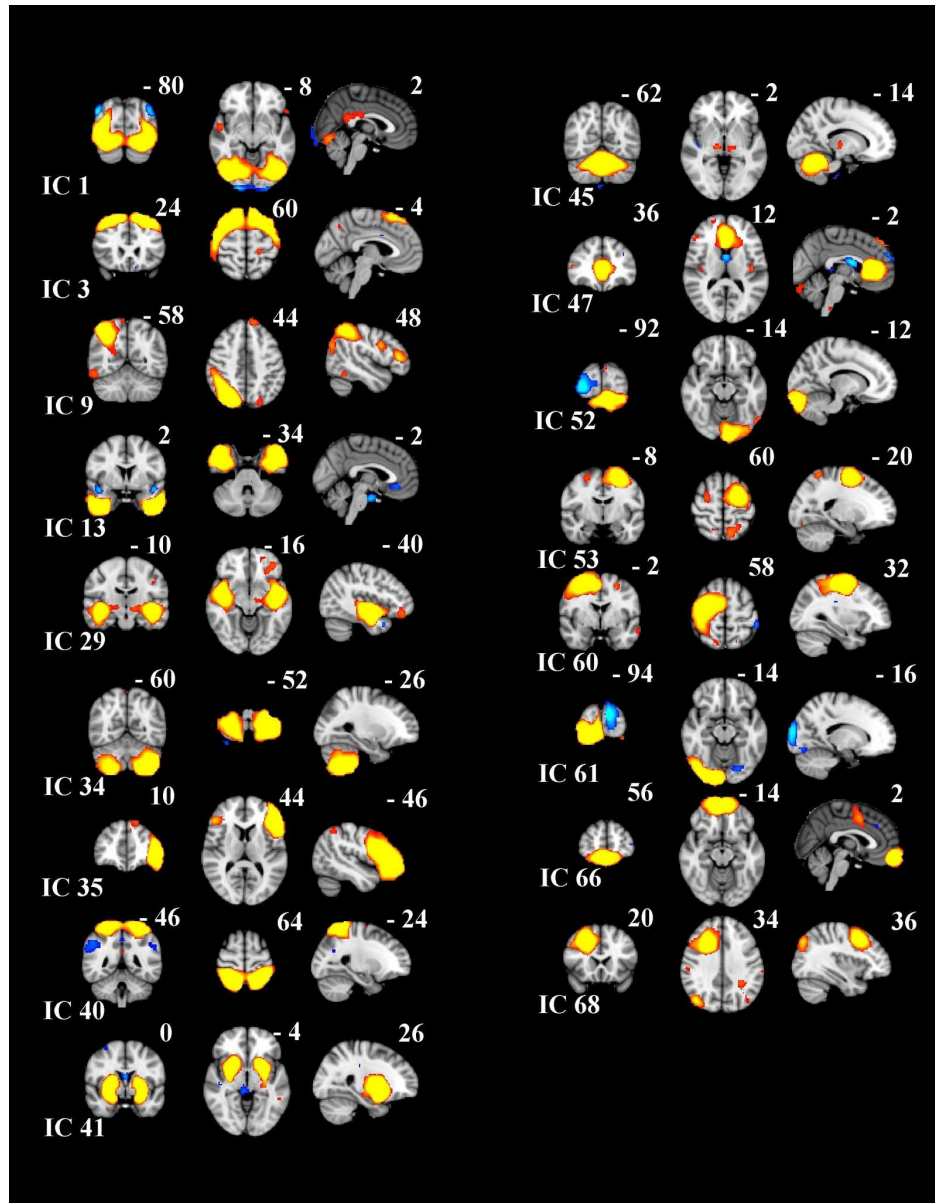
The occipital and parietal RSN signal sources presented in the same way as in Fig.2 with power spectra and rank 1 approximates. The DMN posterior part is depicted in IC 38.
78x124mm (600 x 600 DPI)

1
2
3
4
5
6
7
8
9
10
11
12
13
14
15
16
17
18
19
20
21
22
23
24
25
26
27
28
29
30
31
32
33
34
35
36
37
38
39
40
41
42
43
44
45
46
47
48
49
50
51
52
53
54
55
56
57
58
59
60



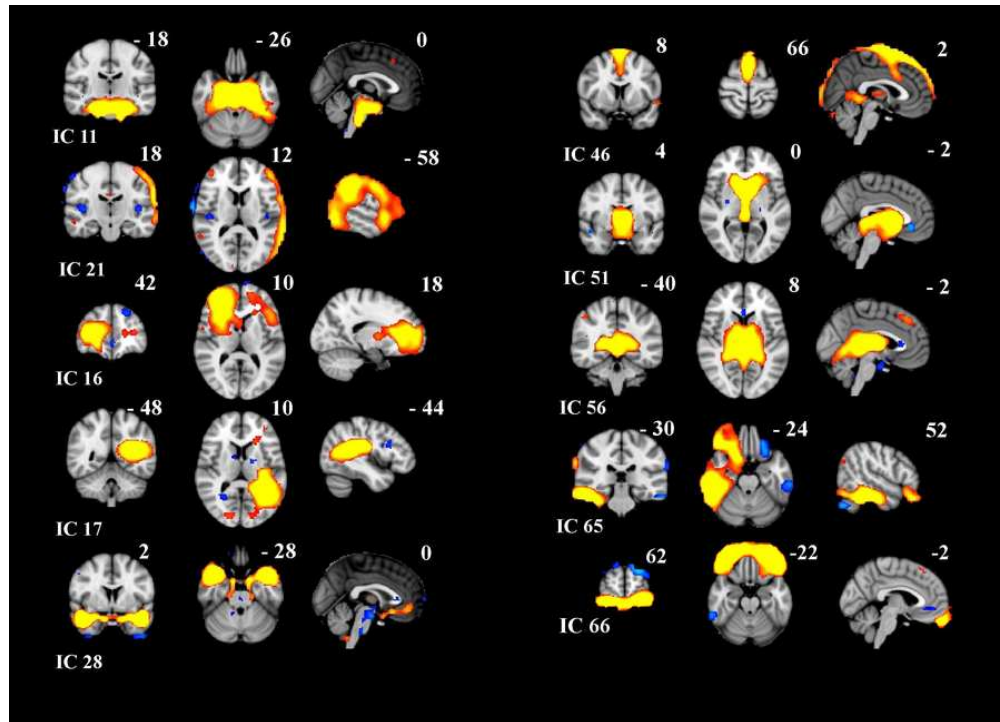
shows examples of frontal signal sources in a similar order to Fig's 2-3. Note the relative lack of power peaks compared to the more posterior components. The default mode network pattern can be seen to originate from several sub-networks in the fused images at the top.
67x80mm (600 x 600 DPI)

1
2
3
4
5
6
7
8
9
10
11
12
13
14
15
16
17
18
19
20
21
22
23
24
25
26
27
28
29
30
31
32
33
34
35
36
37
38
39
40
41
42
43
44
45
46
47
48
49
50
51
52
53
54
55
56
57
58
59
60

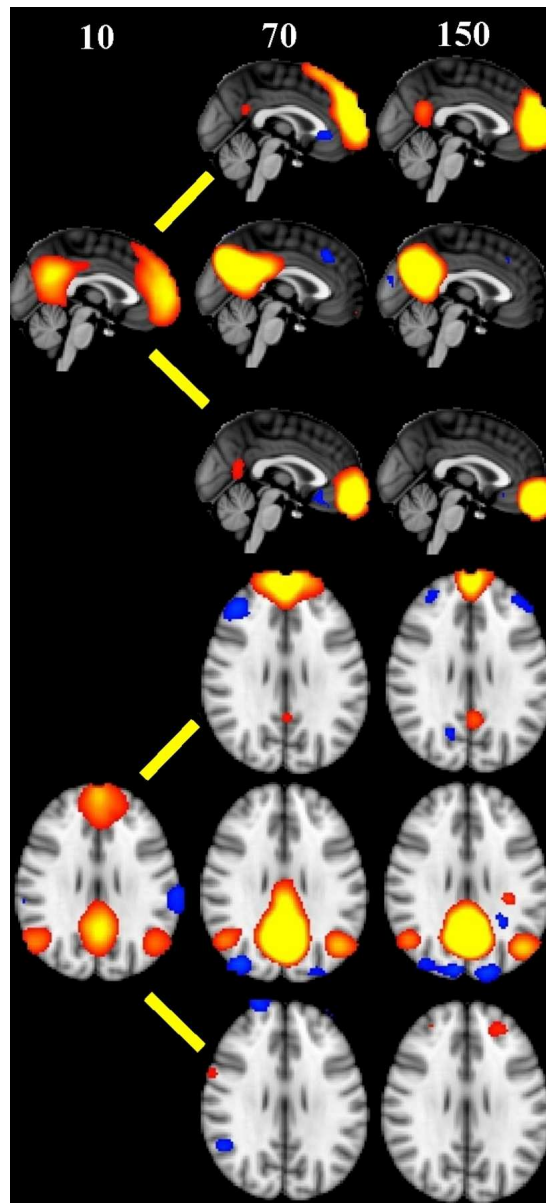


Shows examples of the remaining 17 RSN in coronal, axial and sagittal views on an MNI template. The MNI coordinates are shown in the image. Red-yellow positive z-scores, and blue negative z-scores.

67x86mm (600 x 600 DPI)

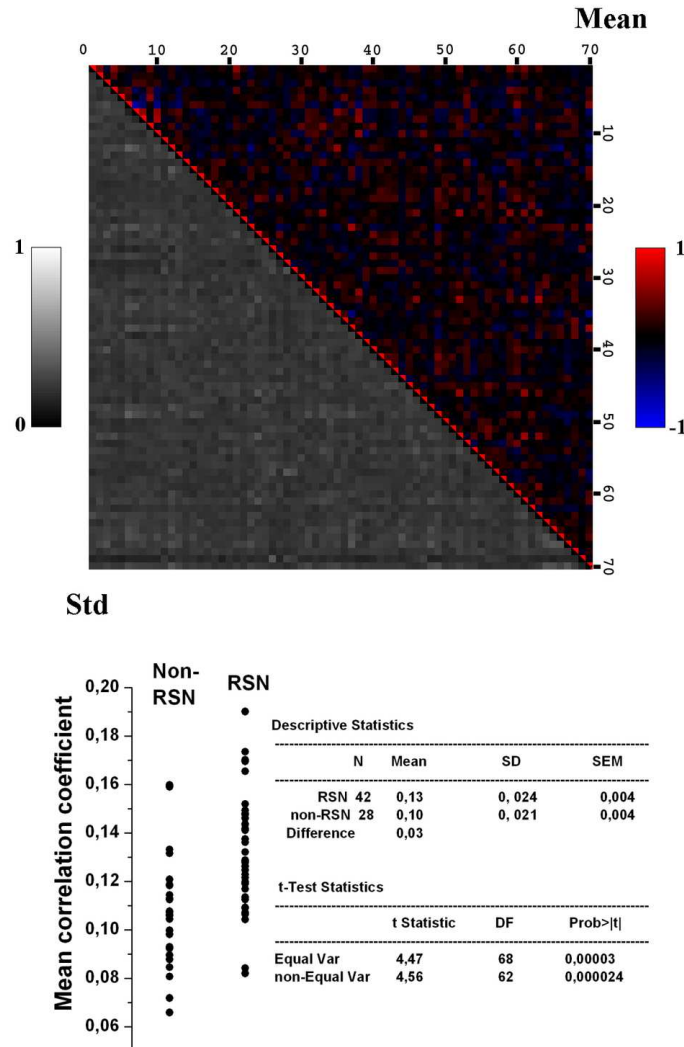


Ten artefactual non-RSN sources, from top left: brain stem pulsation (IC 11), motion artefact (IC18), two white matter sources (IC's 16,17), cerebral artery related (IC 28), Sagital sinus (IC 46), two CSF-ventricle pulsation sources (IC 51,56) and temporal motion related source (IC 65) and frontal sinus susceptibility artefacts (IC 66).
38x27mm (600 x 600 DPI)



Sagittal and axial examples of the default mode network shown with model order 10, 70 and 150 after 100 ICASSO runs shown in a PICA setting in fsl4, with $p = 0.5$ threshold. The core default mode areas become separated into at least three independent sub-networks, one in the pre-cuneus and posterior parietal areas, and two in the ventro-medial prefrontal areas.
34x75mm (600 x 600 DPI)

Inter-source correlation matrix



Top: the individual correlation matrix of each signal source compared to each other enables assessment of the inter-source connectivity of basically the entire brain cortex. Mean correlation coefficients with 0 time lag are color encoded at the top/right, and standard deviations of individual source correlation pairs in grey scale at the bottom. Below: mean inter-component correlation coefficients between individual sources are analysed at the subject level. The resting state network (RSN) components show increased inter-source connectivity between all the calculated sources compared to artefact related non-RSN sources.

42x70mm (600 x 600 DPI)

# IC	ANATOMICAL ROI AREA	Area	Overlap %		t-score		MNI max-t			Template		# ICASSO	Spatial correlation	Iq
			IC vs. ROI		mean	max	X	Y	Z	Source				
1	GM Visual cortex V5	R/L	60/55		6,7 / 5,6	14/11	27/67	31/26	28/31	J	15	0,86	0,964	
	Temporal Occipital Fusiform Cortex		66,5		7,3	20,1	30	29	26	HO				
	Occipital Fusiform Gyrus		78,0		8,1	20,6	30	28	26	HO				
	Lateral Occipital Cortex, inferior division		58,0		6,7	20,1	30	27	26	HO				
2	GM Visual cortex V1 BA17	V1 / V2	37,0 / 37,5		8,5 / 8,6	31,3 / 31,3	60 / 60	16 / 16	34 / 34	J	63	0,84	0,810	
	GM Visual cortex V2 BA18		37,5		8,6	31,3	60,0	16,0	34,0	J				
	Occipital Fusiform Gyrus		55,0		4,9	31,3	60,0	16,0	34,0	HO	50	0,67	0,814	
3	GM Premotor cortex BA6	R/L	30,0 / 31,0		5.83/5.97	13,8 / 13,5	32/54	74/74	66/66	J				
	Superior Frontal Gyrus		43,6		6,9	14,6	30,0	74,0	64,0	HO				
	Middle Frontal Gyrus		42,0		6,8	14,6	30,0	74,0	64,0	HO				
4	GM Visual cortex V5	R/L	73,0 / 62,0		5.9 / 5.4	11. 2 / 9.9	24/64	22/21	42/41	J	61	0,56	0,627	
	Lateral Occipital Cortex, superoir division		44,9		6,8	17,0	52,0	18,0	52,0	HO				
	Cuneal Cortex		55,8		6,8	17,0	52,0	18,0	52,0	HO				
6	GM Anterior intra-parietal sulcus hIP2	R/L	78,0 / 56,0		7,5 / 5,2	18,2 / 12,0	13 / 76	1,0	1,0	J	43	0,83	0,821	
	GM Secondary somatosensory cortex / Parietal operculum OP1		61,5		9,0	19,0	12,0	52,0	54,0	J				
	Supramarginal Gyrus, anterior division		68,8		7,3	19,0	12,0	52,0	54,0	HO				
7	GM Anterior intra-parietal sulcus hIP1		32,9		6,7	17,0	70,0	32,0	50,0	J	46	0,84	0,730	
	GM Visual cortex V5		46,3		5,0	14,4	71,0	29,0	48,0	J				
	Middle Temporal Gyrus, temporooccipital part		38,8		5,2	16,4	73,0	32,0	48,0	HO				
	Angular Gyrus		36,2		6,5	18,0	72,0	32,0	50,0					
8	Frontal Pole		27,2		6,8	21,3	44,0	94,0	46,0	HO	9	0,90	0,950	
	Superior Frontal Gyrus		27,8		7,0	21,0	44,0	94,0	47,0	HO				
	Paracingulate Gyrus		28,6		6,3	18,8	43,0	92,0	48,0	HO				

# IC	ANATOMICAL ROI AREA	Area	Overlap %		t-score		MNI max-t			Template	# ICASSO	Spatial correlation	Iq
			IC vs. ROI	mean	max	X	Y	Z	Source				
9	GM Anterior intra-parietal sulcus HIP1		68,9	6,4	15,5	30,0	28,0	60,0	J	26	0,86	0,914	
	GM Anterior intra-parietal sulcus HIP2		56,7	5,0	10,2	24,0	36,0	62,0	J				
	Lateral Occipital Cortex, superoir division		32,6	6,2	17,5	32,0	26,0	62,0	HO				
10	GM Broca's area BA45		20,6	-1,9	4,1	24,0	82,0	36,0	J	4	0,72	0,982	
	WM Cingulum		20,0	3,0	9,0	50,0	85,0	36,0	J				
	Frontal Medial Cortex		65,3	8,7	22,2	46,0	92,0	32,0	HO				
	Paracingulate Gyrus		50,5	6,5	22,2	46,0	92,0	32,0	HO				
13	GM Amygdala_laterobasal group	R/L	37 / 37	5,6 / 5,1	11,0/9,5	27 / 67	63 / 68	17 / 20	J	8	0,94	0,947	
	GM Hippocampus entorhinal cortex	R/L	40 / 38	5,5 / 4,8	11,5 / 10,0	27 / 62	63 / 60	16 / 16	J				
	Inferior Temporal Gyrus, anterior division		76,7	7,8	14,5	68,0	68,0	16,0	HO				
	Temporal Fusiform Cortex, anterior division		73,8	6,8	13,6	22,0	64,0	16,0	HO				
14	GM Primary somatosensory cortex BA3a	R/L	19,8 / 33,6	5,0 / 5,5	10,8 / 12,8	42 / 51	41 / 44	62 / 60	J	11	0,78	0,939	
	Cingulate Gyrus, posterior division		40,7	6,6	12,9	50,0	44,0	60,0	HO				
	Precuneous Cortex		40,2	5,7	12,9	50,0	44,0	60,0	HO				
	Cuneal Cortex		21,4	3,9	6,4	38,0	32,0	58,0	HO				
			0,0										
15	GM Broca's area BA44	R/L	44,9 / 30,7	4,2 / 4,5	13,0 / 14,6	18 / 67	74 / 75	34 / 32	J	67	0,84	0,579	
	GM Broca's area BA45	R/L	53,1 / 45,5	5,0 / 5,3	13,5 / 15,1	19 / 68	74 / 74	32 / 32	J				
	Inferior Frontal Gyrus, pars tria./operc.		51,0 / 42,6	5,5 / 5,3	15,1 / 14,6	68 / 69	74 / 74	32 / 32	HO				
	Paracingulate Gyrus		43,2	3,9	8,2	46,0	74,0	60,0	HO				
	Frontal Operculum Cortex		66,4	7,6	15,1	68,0	74,0	32,0	HO				
			0,0										
			0,0										
18	GM Primary auditory cortex TE1.1	R/L	44,0 / 64,0	3,3 / 4,1	4,9 / 6,3	24 / 66	48 / 50	44 / 40	J	60	0,72	0,746	
	Paracingulate Gyrus		62,7	6,4	19,0	44,0	76,0	48,0	HO				
	Cingulate Gyrus, anterior division		68,5	7,0	19,0	44,0	76,0	48,0	HO				
19	GM Primary motor cortex BA4a(+p)	R/L	50,2 / 50,8	7,4 / 8,0	15,3 / 15,4	45 / 46	52 / 52	68 / 68	J	35	0,90	0,919	
	GM Primary somatosensory cortex BA3a(+1-3b)	R	41,0 / 39,8	7,8 / 7,7	14,6 / 15,0	44 / 56	50 / 48	66 / 66	J				
	Juxtapositional Lobule Cortex		35,6	7,2	15,4	46,0	52,0	68,0	HO				

# IC	ANATOMICAL ROI AREA	Area	Overlap %		t-score		MNI max-t			Template	# ICASSO	Spatial correlation	Iq
			IC vs. ROI	mean	max	X	Y	Z	Source				
21	GM Visual cortex V1 BA17	V1/V2	55,5 / 51,2	8,7 / 7,7	26,8 / 26,8	42 / 42	18 / 18	36 / 36	J	66	0,91	0,645	
	Intracalcarine Cortex		51,5	10,3	26,8	42,0	18,0	36,0	HO				
	Occipital Pole		52,3	8,3	26,8	42,0	18,0	36,0	HO				
23	GM Anterior intra-parietal sulcus HIP1-2	R/L	47,5 / 38,1	8,0 / 5,6	19,0 / 12,5	20 / 69	34 / 34	59 / 60	J	30	0,81	0,859	
	Supramarginal Gyrus, posterior division		35,2	6,8	19,8	18,0	36,0	58,0	HO				
	Angular Gyrus		50,4	7,8	19,8	18,0	36,0	58,0	HO				
	Lateral Occipital Cortex, superioir division		29,3	5,7	19,8	18,0	36,0	58,0	HO				
24	GM Primary motor cortex BA4a+p	R/L	38,6 / 35,8	7,0 / 5,8	12,7 / 13,5	40 / 50	56 / 57	74 / 74	J	58	0,67	0,907	
	GM Primary somatosensory cortex BA1	R/L	34,4 / 31,1	6,4 / 4,7	12,1 / 11,6	30 / 50	50 / 51	72 / 74	J				
	GM Premotor cortex BA6 R	R/L	27,0 / 27,5	6,6 / 5,8	12,7 / 13,6	40 / 52	56 / 58	74 / 74	J				
	Juxtapositional Lobule Cortex (SMA)		26,0	4,7	13,5	50,0	58,0	74,0	HO				
25	GM Primary auditory cortex TE1.0 (-1.2)	R/L	90,5 / 87,6	8,1 / 8,9	17,7 / 19,3	14 / 76	52 / 50	40 / 40	J	14	0,94	0,925	
	GM Secondary somatosensory cortex / Parietal operculum OP1	R/L	39,7 / 52,9	6,7 / 9,2	17,0 / 19,3	14 / 76	53 / 50	40 / 40	J				
	Heschl's Gyrus (includes H1 and H2)		90,6	8,7	19,4	76,0	50,0	40,0	HO				
27	GM Anterior intra-parietal sulcus HIP2	R/L	49,3 / 48,9	7,0 / 7,9	17,9 / 18,7	22 / 70	50 / 48	63 / 61	J	69	0,88	0,578	
	GM Primary motor cortex BA4p (+a)		35,3	7,9	18,3	22,0	51,0	64,0	J				
	GM Primary somatosensory cortex BA2	R/L	55,6 / 59,8	7,6 / 9,9	18,3 / 19,8	22 / 66	52 / 52	64 / 66	J				
	Supramarginal Gyrus, anterior division		56,3	6,4	19,3	68,0	48,0	63,0	HO				
29	GM Amygdala_centromedial group	R/L	68,6 / 40,1	5,0 / 4,5	11,6 / 9,6	24 / 62	61 / 54	26 / 31	J	23	0,90	0,940	
	GM Hippocampus cornu ammonis	R/L	41,0 / 32,6	5,2 / 5,3	12,9 / 13,7	24 / 65	57 / 54	29 / 30	J				
	GM Lateral geniculate body	R/L	54,4 / 42,7	3,5 / 3,4	5,8 / 5,7	30 / 60	55 / 53	32 / 30	J				
	Planum Polare		64,5	7,7	15,6	66,0	56,0	30,0	HO				
30	GM Anterior intra-parietal sulcus HIP1	R/L	37,9 / 21,6	3,8 / 3,7	6,2 / 5,8	26 / 24	34 / 36	60 / 60	J	33	0,84	0,923	
	GM Broca's area BA44 (+BA45)	R/L	77,5 / 33,9	6,7 / 4,4	13,1 / 8,3	20 / 68	70 / 72	48 / 48	J				
	GM Secondary somatosensory cortex / Parietal operculum OP3 (+OP2,4)	R	55,3	4,5	10,5	22,0	65,0	46,0	J				
	Inferior Frontal Gyrus, pars opercularis		63,9	6,3	13,1	20,0	70,0	48,0	HO				
	Right Caudate		20,0	3,1	4,2	34,0	61,0	46,0	HO				

# IC	ANATOMICAL ROI AREA	Area	Overlap %		t-score		MNI max-t			Template	# ICASSO	Spatial correlation	Iq
			IC vs. ROI	mean	max	X	Y	Z	Source				
31	GM Broca's area BA45	R/L	16,7 / 29,0	0,4 / 4,0	7,4 / 11,1	22 / 66	86 / 86	45 / 43			54	0,69	0,665
	Frontal Pole		42,5	5,1	18,6	60,0	94,0	40,0					
	Inferior Frontal Gyrus, pars triangularis		22,3	1,5	8,8	66,0	84,0	45,0					
32	GM Hippocampus subiculum	R/L	42,9 / 48,2	4,8 / 5,4	9,4 / 11,02	32 / 58	42 / 43	30 / 30	J		28	0,66	0,936
	GM Visual cortex V2 BA18		26,0	3,4	9,9	52,0	34,0	38,0	J				
	GM Medial (+lateral) geniculate body	R/L	55,8 / 88,5	3,4 / 3,9	4,9 / 6,2	38 / 50	47 / 46	29 / 30	J				
	Parahippocampal Gyrus, posterior division		83,3	5,7	12,0	58,0	42,0	28,0	HO				
34	Cerebellum										13	0,91	0,935
35	GM Broca's area BA45(+BA45)	R/L	19,4 / 97,0	3,5 / 8,8	5,6 / 17,7	20 / 70	80 / 84	40 / 36	J		42	0,84	0,811
	Inferior Frontal Gyrus, pars triangularis		59,6	8,0	17,7	70,0	84,0	36,0	J				
	Inferior Frontal Gyrus, pars opercularis		51,5	6,7	16,5	70,0	78,0	41,0	J				
	Frontal Operculum Cortex		39,7	5,8	15,6	70,0	77,0	41,0	J				
37	Frontal Pole		32,2	4,5	15,7	28,0	84,0	54,0	HO		34	0,69	0,897
	Superior Frontal Gyrus		27,5	3,9	15,7	28,0	84,0	54,0	HO				
	Middle Frontal Gyrus		36,9	5,5	15,7	28,0	84,0	54,0	HO				
	Paracingulate Gyrus		22,9	1,0	5,1	41,0	90,0	53,0	HO				
38	Cingulate Gyrus, posterior division		50,5	8,2	19,7	46,0	33,0	50,0	HO		65	0,83	0,883
	Precuneous Cortex		43,8	8,0	19,9	46,0	32,0	50,0	HO				
	Cuneal Cortex		40,2	8,4	19,7	46,0	31,0	50,0	HO				
	Supracalcarine Cortex		53,6	9,2	19,9	46,0	32,0	50,0	HO				
39	GM Visual cortex V5	R/L	91,5 / 56,0	7,1 / 4,0	12,7 / 6,2	18 / 70	34 / 32	38 / 36	J		16	0,86	0,923
	Middle Temporal Gyrus, temporooccipital part		69,4	6,4	14,6	20,0	38,0	38,0	J				
	Inferior Temporal Gyrus, temporooccipital part		37,7	5,9	13,3	17,0	37,0	36,0	J				
	Lateral Occipital Cortex, inferior division		34,2	5,3	13,6	20,0	36,0	38,0	J				

# IC	ANATOMICAL ROI AREA	Area	Overlap %		t-score		MNI max-t			Template	# ICASSO	Spatial correlation	Iq
			IC vs. ROI	mean	max	X	Y	Z	Source				
40	GM Primary somatosensory cortex BA2	R/L	36,8 / 39,0	5,6 / 6,4	15,0 / 12,7	32 / 58	36 / 36	70 / 70	J	20	0,82	0,908	
	Postcentral Gyrus		22,1	5,2	14,9	33,0	36,0	70,0	HO				
	Superior Parietal Lobule		52,1	6,1	15,0	32,0	36,0	70,0	HO				
	Lateral Occipital Cortex, superioir division		20,3	5,6	15,0	32,0	36,0	70,0	HO				
	Precuneous Cortex		17,8	3,4	13,7	37,0	34,0	70,0	HO				
41	GM Amygdala_centromedial group	R/L	80,1 / 76,3	6,9 / 6,2	18,4 / 14,6	31 / 58	64 / 63	32 / 32	J	12	0,93	0,942	
	Putamen	R/L	92,7 / 93,4	9,4 / 7,9	21,0 / 18,4	58 / 32	66 / 66	34 / 32	HO				
	Pallidum		80,0 / 80,4	5,5 / 7,0	11,4 / 16,9	56 / 54	66 / 70	34 / 33	HO				
	Accumbens	R/L	51,4 / 55,7	5,4 / 5,5	12,3 / 11,4	36 / 54	70 / 70	32 / 33	HO				
43	GM Primary auditory cortex TE1.2	R/L	59,9 / 43,5	9,9 / 8,7	26,2 / 23,5	14 / 74	60 / 58	43 / 45	J	1	0,95	0,984	
	GM Primary somatosensory cortex BA3b	R/L	37,2 / 37,2	14,0 / 13,4	34,1 / 33,7	16 / 72	60 / 58	48 / 50	J				
	GM Secondary somatosensory cortex / Parietal operculum OP4 (OP1-3)	R/L	72,9 / 71,9	12,2 / 12,3	34,1 / 33,7	16 / 72	60 / 58	48 / 50	J				
	Central Opercular Cortex		39,3	10,0	30,7	16,0	60,0	46,0	HO				
45	GM Medial geniculate body	R/L	24,7 / 16,4	3,0 / 3,0	3,5 / 3,5	38 / 49	52 / 48	33 / 30	J	17	0,90	0,901	
	Brain-Stem		22,3	4,2	11,1	42,0	40,0	24,0	HO				
	Right Thalamus		8,5	3,3	4,3	40,0	52,0	34,0	HO				
47	GM Primary auditory cortex TE1.2	R/L	31,2/43,7	4,5/4,5	7,9/7,8	22	60	36	J	47	0,82	0,795	
	Subcallosal Cortex		29,0	6,6	16,4	44	78	38	HO				
	Paracingulate Gyrus		31,7	5,7	16,4	44	81	38	HO				
	Cingulate Gyrus, anterior division		33,8	6,8	17,1	44	80	38	HO				
	Left Accumbens		31,4	4,4	8,6	48	74	36	HO				
49	GM Broca's area BA44	R/L	53,5 / 41,1	5,3 / 1,8	12,9 / 10,2	16 / 74	66 / 64	36 / 36	J	57	0,65	0,586	
	GM Primary auditory cortex TE1.2	R/L	99,8 / 91,0	7,6 / 5,6	13,0 / 10,2	16 / 74	66 / 64	36 / 36	J				
	Insular Cortex		59,7	5,4	12,7	24,0	66,0	36,0	J				
	Juxtapositional Lobule Cortex (SMA)		57,9	4,9	11,4	44,0	66,0	58,0	HO				
	Frontal Operculum Cortex		62,0	6,0	13,0	16,0	66,0	36,0	HO				
	Central Opercular Cortex		65,2	6,1	13,0	16,0	66,0	36,0	HO				
	Planum Polare		69,8	6,3	13,0	16,0	66,0	36,0	HO				

# IC	ANATOMICAL ROI AREA	Area	Overlap %		t-score		MNI max-t			Template	# ICASSO	Spatial correlation	Iq
			IC vs. ROI	mean	max	X	Y	Z	Source				
52	GM Visual cortex V1 BA17	L , V1/V2	19,7 / 19,4	1,7 / 1,6	16,6 / 15,8	54 / 52	18 / 18	24 / 25	J	32	0,73	0,888	
	Lateral Occipital Cortex, inferior division	L	24,5	3,6	17,1	56,0	20,0	24,0	J				
	Occipital Fusiform Gyrus	L	34,7	5,9	17,1	56,0	20,0	24,0	HO				
	Occipital Pole	L	28,1	1,7	17,0	52,0	18,0	24,0	HO				
53	GM Primary motor cortex BA4a	L	18,9	4,5	10,5	60,0	58,0	62,0	J	41	0,30	0,942	
	Superior Frontal Gyrus		19,7	5,5	12,2	58,0	60,0	64,0	HO				
	Middle Frontal Gyrus		14,2	5,5	12,2	58,0	60,0	64,0	HO				
	Juxtapositional Lobule Cortex (SMA)		25,8	4,1	7,9	53,0	64,0	64,0	HO				
59	GM Visual cortex V1 BA17		55,5	9,7	22,3	50,0	28,0	38,0	J	10	0,88	0,951	
	GM Visual cortex V2 BA18	R	54,4	9,3	22,3	50,0	28,0	38,0	J				
	Intracalcarine Cortex	R	86,9	12,0	22,3	50,0	28,0	38,0	HO				
	Lingual Gyrus	R	63,1	10,4	22,3	50,0	28,0	38,0	HO				
	Supracalcarine Cortex	R	68,6	11,6	22,3	50,0	28,0	38,0	HO				
60	GM Anterior intra-parietal sulcus hIP2	R	49,4	4,4	8,4	25,0	51,0	62,0	J	52	0,79	0,678	
	GM Primary motor cortex BA4p	R	47,9	5,5	11,0	33,0	56,0	64,0	J				
	GM Primary somatosensory cortex BA2	R	50,0	4,6	9,1	24,0	53,0	64,0	J				
	GM Premotor cortex BA6	R	55,1	6,1	13,8	32,0	60,0	64,0	J				
61	GM Visual cortex V1 BA17	R	23,8	2,8	16,5	36,0	18,0	26,0	J	55	0,64	0,627	
	GM Visual cortex V2 BA18		22,4	2,7	16,6	32,0	20,0	26,0	J				
	Occipital Fusiform Gyrus		33,7	5,8	16,7	32,0	20,0	24,0	HO				
	Occipital Pole		32,0	3,9	16,6	32,0	20,0	25,0	HO				
63	Lateral Occipital Cortex, superior division		21,3	6,0	25,0	43,0	24,0	58,0	J	61	0,61	0,628	
	Precuneous Cortex		30,9	8,1	25,1	44,0	24,0	56,0	J				
	Cuneal Cortex		54,0	8,9	25,1	44,0	24,0	56,0	J				
	Supracalcarine Cortex		29,7	6,7	23,2	42,0	25,0	56,0	J				
66	Frontal Medial Cortex		33,9	6,6	15,2	42	94	28		4	0,70	0,971	

1
2
3
4
5
6
7
8
9
10
11
12
13
14
15
16
17
18
19
20
21
22
23
24
25
26
27
28
29
30
31
32
33
34
35
36
37
38
39
40
41
42
43
44
45
46
47

# IC	ANATOMICAL ROI AREA	Area	Overlap %	t-score		MNI max-t			Template	# ICASSO	Spatial correlation	Iq
			IC vs. ROI	mean	max	X	Y	Z	Source			
	Juxtapositional Lobule Cortex (SMA)		25,7	3,4	5,2	48	64	58				
	Middle Temporal Gyrus, temporooccipital part		19,6	3,6	6,0	72	36	40				
68	GM Broca's area BA44		20,7	4,6	24,5	29,0	68,0	56,0	J	68	0,70	0,602
	GM Primary auditory cortex TE1.2		24,4	3,1	74,7	78,0	53,0	42,0	J			
	GM Visual cortex V5		33,2	3,6	19,2	20,0	28,0	47,0	J			
	Superior Frontal Gyrus		21,8	5,6	33,6	32,0	70,0	56,0	HO			
										max	0,95	0,984
										mean	0,79	0,829
										std	0,13	0,132

#IC = number of selected component, Anatomical ROI Area = Name of anatomical template from fsl4, Area = side or other anatomical specification R = right, L= left, Overlap % = anatomical overlap percentage of components vs. anatomical structure, t-score = t-value (mean, maximum [Max], minimum[Min]), MNI max-t = maximum t-value x, y & z-direction Montreal Neurologic Institute 152 coordinates, Template source = anatomical ROI source in fsl4: J= Juelich, HO=Harvard-Oxford template, # ICASSO = icasso run equivalent to selected IC, spatial correlation = spatial correlation between ICASSO and selected IC, Iq = ICASSO clustering index.